

國立交通大學

電子物理學系

碩士論文

半導體奈米晶體與奈米柱系統之少電子理論



Few-Electron Theory of Semiconductor

Nanocrystal and Nanorod Systems

研究生：陳彥廷

指導教授：鄭舜仁 教授

中華民國九十六年七月

半導體奈米晶體與奈米柱系統之少電子理論

Few-Electron Theory of Semiconductor

Nanocrystal and Nanorod Systems

研究生：陳彥廷

Student：Yan-Ting Chen

指導教授：鄭舜仁

Advisor：Shun-Jen Cheng

國立交通大學

電子物理學系



A Thesis

Submitted to Department of Electrophysics

College of Science

National Chiao Tung University

in partial Fulfillment of the Requirements

for the Degree of

Master in Science

July 2007

Hsinchu, Taiwan, Republic of China

中華民國九十六年七月

誌 謝

本篇論文得以順利完成，作者必須要感謝許多人。感謝我的父母 陳貴華先生及 楊娟娟女士多年來的辛苦栽培，令我有機會在交大學習與研究。感謝我的指導教授 鄭舜仁老師兩年半來無私且耐心的教導，他傳授給我的知識、方法與觀念令我終生受用。感謝我的同窗好友張志彬同學這兩年來各方面的幫助。感謝盧書楷學長、黃上瑜學弟、張志豪學弟、趙虔震學弟、洪瑞甫學弟、陳勇達學弟這段日子的陪伴。最後必須感謝交大竹韻口琴社，令我在交大的這六年過得非常豐富愉快。




半導體奈米晶體與奈米柱系統之少電子理論

學生：陳彥廷

指導教授：鄭舜仁 教授

國立交通大學電子物理學系(研究所)碩士班

摘要



本論文旨在建立一套針對奈米晶體/奈米柱系統之少體理論方法。我們採用三維的拋物線型位能模型，模擬並計算電子的運動行為與能譜結構。拋物線型位能兼具簡單、可與外加磁場偶合并解析、可在非等向系統中解析等優點，已在解釋二維系統中得到巨大的成功。首先我們分別計算單電子在(1)等向奈米晶體、(2)等向奈米晶體外加磁場以及(3)非等向之奈米柱等系統中之能譜結構；之後經由引入庫倫交互作用項，我們依據組態交互作用法建構少個電子的多體理論，此理論可以計算少量電子在這些奈米系統中的能譜及電子結構。在組態交互作用法中，我們選取有限數量的組態當作基底並依此基底建構系統的漢密頓矩陣，透過對角化漢密頓矩陣我們可以得到系統(在此有限組態近似下)的本徵能量與本徵態。最後，在兩個殼層的近似下，我們實際計算一個雙電子的奈米晶體/奈米柱系統，並且印證透過外加磁場及改變系統形狀來調控系統電子結構的可行性。

Few-Electron Theory of Semiconductor Nanocrystal and Nanorod Systems

Student: Yan-Ting Chen

Advisor: Shun-Jen Cheng

Department of Electrophysics
National Chiao Tung University

ABSTRACT

The purpose of this thesis is to develop a configuration interaction (CI) method for studying the few-body physics of interacting charged nanocrystal (NC) and nanorod (NR) systems. In the framework of the effective mass approximation, we develop a CI theory based on a three-dimensional (3D) parabolic model for the calculation of the few-electron spectrum of crystalline semiconductor nanoparticles with a size comparable to the effective Bohr radius. We derive the explicit formulation of the Coulomb matrix elements required in the theory and conducted the evaluations in a simple semi-analytical manner. We then apply this theory to three simple representative cases: (1) two mutually interacting electrons in a symmetric NC without a magnetic field, (2) two mutually interacting electrons in a symmetric NC under an external magnetic field, and (3) two mutually interacting electrons in an oblate or a prolate NC (NR) in the absence of a magnetic field. We calculate the ground states and the energy spectrum of two interacting electrons in nanosystems using the partial CI approach within the simple two-shell approximation and explore the possibility of singlet/triplet (S/T) state transitions, a physical phenomenon as the manifestation of particle-particle interaction, driven by magnetic fields and/or shape deformation.

目 錄 (Contents)

中文摘要	i
Abstract	ii
Contents	iii
Chapter 1 Introduction	1
Chapter 2 Model	4
2.1 3D Isotropic Parabolic Model	4
2.2 3D Anisotropic Parabolic Model	16
Chapter 3 Configuration Interaction Theory for Nanocrystal/Nanorods (NC/NRs)	19
Chapter 4 Results	23
4.1 Two Electrons in an Isotropic NC without a Magnetic Field	23
4.2 Two Electrons in an Isotropic NC in Magnetic Fields	26
4.3 Two Electrons in an Anisotropic NC (NR)	29
Chapter 5 Summary	33
Appendix Coulomb Matrix Elements	35
References	41



Chapter 1: Introduction

Semiconductor nanocrystals (NCs) are chemically synthesized crystallite semiconductor nanoparticles with sizes comparable to or even smaller than the effective Bohr radius [1, 2]. The size effects of nanostructures lead to the strong quantization of the electronic structure at an energy level typically above 100 meV; further, due to these effects, the material and physical properties of nanostructures significantly differ from those of the bulk systems. NCs have novel properties and therefore they are widely used as promising nanomaterials for various applications in many fields from optoelectronics to biotechnology [3, 4]. Remarkably, as compared with other nanostructures, NCs are particularly advantageous in the engineering of electronic structures by shape and size control. The sizes of NCs can be controlled over a wide range of diameters, typically from 1 to 10 nm, by delicate fabrication processes [5]. Significant effects of size on the optical properties of NCs have been explored over the years and used for the application of advanced light sources [6]. Moreover, NCs can be synthesized in various shapes, from spherical nanoparticles (quasi-0D system) to elongated nanorods (quasi-1D system), thereby providing a unique platform for studying various intriguing physical phenomena of low-dimensional systems.

Although NCs have been used in applications such as optoelectronic devices and biological fluorescence marking, direct measurements of the electronic structures of individual NCs have remained a challenging task for many years. Only the recent advances in tunneling spectroscopy based on STM techniques [7, 8] have enabled the measurement of the addition energy spectrum of the conduction and valence bound states in an *individual* NC. The polarized optical emission spectra of single NRs and NCs have also been revealed recently by using an advanced technique known as single-dot optical spectroscopy [9, 10].

Theoretically, the electronic structure and the optical spectrum of NCs have been investigated

by using different approaches such as the effective mass approximation, multiband $k \cdot p$ model, tight-binding theory, and the pseudopotential theory. Rodina, Efros, and Alekseev have studied the structure of electron quantum size levels in spherical NCs in the framework of an eight-band effective-mass $k \cdot p$ model [11]. Chen has determined the Zeeman splitting of electrons and holes in semiconductor nanostructures using the empirical tight-binding method [12]. Franceschetti and Zunger have calculated the dependence of the optical transitions in CdSe nanocrystals based on single-electron pseudopotential wave functions [13].

In this thesis, we focus on the studies of the electronic structure and few-body physics in NC/NR systems in the framework of the effective mass approximation. We develop a configuration interaction (CI) theory based on a three-dimensional (3D) simple harmonic oscillation (SHO) model for NC/NR systems containing interacting electrons. In Table 1, we list some relevant parameters of the 3D SHO model used for NCs/NRs. The interplay between the few-body physics and the electronic structure of semiconductor nanostructures has been extensively explored in Coulomb blockade spectroscopy for gate-defined two-dimensional (2D) quantum dots (QDs) under magnetic fields [14, 15]. The applied magnetic fields are used as a tuning parameter for the engineering of electronic structures and Coulomb interaction strength and allows for studying few-body physics on the test bed of QD systems in a systematic manner. Rich, interesting, and significant physical phenomena such as the integer/fractional quantum Hall effect (QHE), magic numbers in the addition energy spectrum, subsequent formation of the maximum-density droplet and its reconstruction, and spin singlet-triplet transition have been revealed in the measurement of the magnetospectrum of QDs. It is remarkable that the S/T state transition of a two-electron complex in a QD is identified at some finite magnetic fields as the manifestation of the spin-spin exchange interaction between electrons. For a QD charged with many electrons and high magnetic fields, a rich pattern of Coulomb blockade current peaks has been observed between the filling-factor states 2 and 1, corresponding to a series of spin flips driven by correlation

interaction further enhanced by the magnetic fields [16, 17, 18]. Hence, we attempt to explore the few-body physics in 3D QDs, i.e., NCs and NRs, whose electronic structures can be tuned either by magnetic fields or by shape control.

This thesis is organized as follows. In Chapter 2, we describe the single particle behavior in a nanocrystal or a nanorod with/without the application of a magnetic field within the 3D SHO parabolic model. In Chapter 3, we describe the configuration interaction (CI) method for NC/NR systems and apply the theory to a simple representative case: two interacting electrons in a spherically symmetric NC with magnetic fields. In Chapter 4, we describe the calculated results for two electrons in asymmetric nanocrystals in magnetic fields by using the developed CI theory within the 2-shell approximation.

r	2D Dots			3D		
	1 μ m	100 nm	10 nm	100 nm	10 nm	1 nm
$\hbar\omega_0$	0.294 μ eV	29.37 μ eV	2.94 meV	29.37 μ eV	2.94 meV	293.69 meV
V_0	0.106 meV	1.06 meV	10.63 meV	0.34 meV	3.38 meV	33.81 meV
V_0/ω_0	360.54	36.05	3.62	11.56	1.15	0.12
$\omega_c/\omega_0=1 \rightarrow B(\text{T})$	0.33 mT	33 mT	3.3 T	33 mT	3.3 T	329.99 T

Table 1. Some relevant parameters of 2D/3D SHO systems as a model of CdSe (where the electron effective mass $m^* = 0.13$) nanostructures. Here, $r \equiv \sqrt{\langle r^2 \rangle}$, $\hbar\omega_0$, V_0 , and ω_c indicate the size, quantization energy, Coulomb interaction strength of the NC, and cyclotron frequency reflecting the external magnetic field strength, respectively. $\omega_c/\omega_0=1$ corresponds to a different value of magnetic field. Throughout this thesis we focus on 3D NCs with $r = 1 \sim 5$ nm in the regime where the energy is of the order of a few hundred electron volts.

Chapter 2: Model

3D Parabolic Model

In this chapter, we discuss the energy spectrum of a single electron subjected to an isotropic and/or anisotropic 3D parabolic confining potential, a model potential suitable for NC and NR systems in the framework of the effective mass approximation. In the CI theory developed in Chapter 3, the single electron states are used for the construction of many-electron configurations for the interacting electrons in NCs. Here, let us first review three known approaches for solving the single electron Schrödinger equation of a 3D SHO system:

$$\hat{H} = \frac{\mathbf{p}^2}{2m^*} + \frac{1}{2}m^* (\omega_x^2 x^2 + \omega_y^2 y^2 + \omega_z^2 z^2), \quad \text{Eq. (2.0.1)}$$

where \mathbf{p} is the momentum operator, m^* is the effective mass of the electron, $\vec{r} = (x, y, z)$ is the coordinate position of the electron, and ω_α ($\alpha = x, y, z$) is the characteristic frequency of the parabolic confining potential along each direction. The physical quantities in this thesis are all in **SI** unit if there's no exceptional note.

The three approaches help us to gain a physical understanding of the single-electron problem from the perspectives of the 3D SHO, 3D central force problem, and circular oscillation. For transparency, we first discuss the isotropic cases. However, the theory can be extended to cases with an applied magnetic field and shape anisotropy.

2.1 3D Isotropic Parabolic Model

Perspective of simple harmonic oscillation

The first method for solving Eq. (2.0.1) is to treat the 3D Schrödinger equation separable, i.e.,

$$\hat{H} = \left(\frac{p_x^2}{2m^*} + \frac{1}{2}m^* \omega_0^2 x^2\right) + \left(\frac{p_y^2}{2m^*} + \frac{1}{2}m^* \omega_0^2 y^2\right) + \left(\frac{p_z^2}{2m^*} + \frac{1}{2}m^* \omega_0^2 z^2\right) = \hat{H}_x + \hat{H}_y + \hat{H}_z, \quad \text{Eq. (2.1.1)}$$

and take the form of the wave function as

$$|\psi_{n_x, n_y, n_z}\rangle = |\psi_{n_x}\rangle \otimes |\psi_{n_y}\rangle \otimes |\psi_{n_z}\rangle. \quad \text{Eq. (2.1.2)}$$

Following the standard SHO quantum theory, we have the eigenenergy

$$E_n = (n + \frac{3}{2})\hbar\omega_0, \quad \text{Eq. (2.1.3)}$$

and the single electron wave function

$$|\psi_{n_x, n_y, n_z}\rangle = \frac{1}{\sqrt{n_x! n_y! n_z!}} (a_x^+)^{n_x} (a_y^+)^{n_y} (a_z^+)^{n_z} |0, 0, 0\rangle, \quad \text{Eq. (2.1.4)}$$

$$\text{where } a_k = \sqrt{\frac{m\omega_0}{2\hbar}}k + \frac{i}{\sqrt{2m\hbar\omega_0}}p_k,$$

$$a_k^+ = \sqrt{\frac{m\omega_0}{2\hbar}}k - \frac{i}{\sqrt{2m\hbar\omega_0}}p_k.$$

($k = x, y, z$)

$$n = n_x + n_y + n_z \quad (n_x, n_y, n_z = 0, 1, 2, \dots).$$

In the SHO picture, we can easily identify the amplitude and energy of electron motion, in terms of the quantum numbers n_x , n_y , and n_z , oscillating in each direction (x, y, and z).

The method is applicable even for anisotropic ($\omega_x \neq \omega_y \neq \omega_z$) systems. However, the zero-field SHO basis in Cartesian coordinates cannot describe electrons that move circularly in the presence of a magnetic field and it is inappropriate for the system under the influence of a magnetic field. Moreover, some important physical variables related to electron motion, such as the angular momentum, in a QD system are not explicitly expressed in the formulation.

Spherical potential model

The second method is to treat the problem as a general spherical potential problem. Following the standard procedure for solving the differential equation of a 3D spherical potential system, we separate the wave function into a radial part and an angular part that is known as the

spherical harmonic function. By substituting the wave function into the Schrödinger equation, we have

$$H\psi(\vec{r}) = H(R_{N,L}(r)Y_L^M(\theta, \phi)) = E(R_{N,L}(r)Y_L^M(\theta, \phi)), \quad \text{Eq. (2.1.4),}$$

The equation can be simplified as

$$\left[-\frac{\hbar^2}{2m^*} \frac{1}{r} \frac{d^2}{dr^2} r + \frac{1}{2} m^* \omega_0^2 r^2 + \frac{L(L+1)\hbar^2}{2m^* r^2} \right] R_{N,L}(r) = ER_{N,L}(r) \quad \text{Eq. (2.1.5),}$$

which is an ordinary differential equation and can be solved by the power series method.

By taking the power series expansion of the undetermined radial wave function and substituting it into the above equation, we can obtain a recurrence relation. From the relation, we could determine the relationship between the principle quantum number N and the angular quantum number L . In this picture, the eigenenergy can be represented as

$$E = (N + \frac{3}{2})\hbar\omega \quad \text{Eq. (2.1.6).}$$

A plot of the energy spectrum against the total angular momentum is shown in FIG. 2.1.1. In the lowest shell (termed s-shell), N is equal to 0, L can only be 0, and there is no degeneracy in this energy level. In the p-shell, N is equal to 1 and L can only be 1; thus, there are three degenerate states corresponding to different magnetic quantum numbers $M = 1, 0, \text{ and } -1$ in the same energy level. Furthermore, in the d-shell, L could be 0 or 2 and there are 5 degenerate states while $L = 2$ and so on.

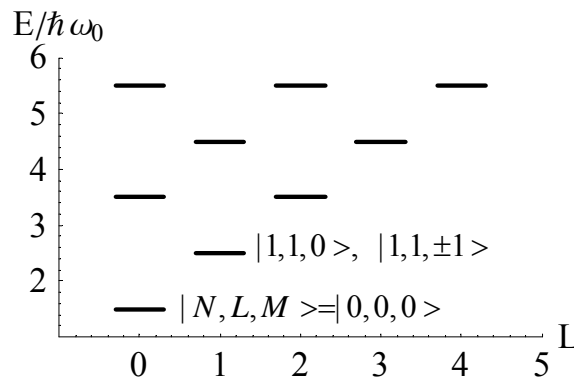


FIG. 2.1.1 Energy spectrum versus total angular momentum. The degeneracy is indicated in the three lowest shells.

In the perspective of the power series method, the relation between the energy levels and the angular momentum (and the degeneracy in each level) is evident. However, this method cannot be used for anisotropic systems. In this thesis, the two methods mentioned above are inappropriately used to determine the single electron states as the basis of the many-body theory for isotropic/anisotropic NCs in magnetic fields. The third approach introduced below would be suitable for this purpose.

Perspective of a 3D SHO system in the circular basis

Let us consider a 3D SHO system subjected to an external magnetic field $\mathbf{B} = B\hat{\mathbf{z}}$ along the z-axis. The corresponding Hamiltonian is

$$\hat{H} = \frac{1}{2m^*} \left(\mathbf{p} - \frac{e}{c} \mathbf{A} \right)^2 + \frac{1}{2} m^* \omega_0^2 r^2 \quad \text{Eq.(2.1.7),}$$

where $\mathbf{A} = \left(-\frac{By}{2}, \frac{Bx}{2}, 0 \right)$ is the vector potential in the symmetric gauge. Due to the external magnetic field, the two oscillators on the plane normal to the B-field are coupled to each other, while the oscillator in the z-direction is still independent of the other two. Here, we introduce the following operators for creating/annihilating the modes of the circular in-plane motion and SHO motion in the z-direction:

$$\begin{aligned} a &= \frac{1}{2} \left(\frac{x-iy}{\sqrt{2l}} + \sqrt{2l}(\partial_x - i\partial_y) \right), \quad a^+ = \frac{1}{2} \left(\frac{x+iy}{\sqrt{2l}} - \sqrt{2l}(\partial_x + i\partial_y) \right) \\ b &= \frac{1}{2} \left(\frac{x+iy}{\sqrt{2l}} + \sqrt{2l}(\partial_x + i\partial_y) \right), \quad b^+ = \frac{1}{2} \left(\frac{x-iy}{\sqrt{2l}} - \sqrt{2l}(\partial_x - i\partial_y) \right) \\ a_z &= \frac{z}{2l_z} + l_z \partial_z, \quad a_z^+ = \frac{z}{2l_z} - l_z \partial_z \end{aligned} \quad \text{Eq. (2.1.8),}$$

where the confining length defined as

$$\begin{aligned} l &= \sqrt{\hbar / 2m\omega_h}, \\ l_z &= \sqrt{\hbar / 2m\omega_z}, \end{aligned}$$

Using Eq. (2.1.8), the eigenstates $|n, m, q\rangle$ are expressed as

$$|n, m, q\rangle = (a^+)^n (b^+)^m (a_z^+)^q |000\rangle \quad \text{Eq. (2.1.9),}$$

where $n, m,$ and $q = 0, 1, 2, \dots$ (instead of $n_x, n_y,$ and n_z).

The eigenenergy in the basis is expressed as

$$E = \hbar\omega_+ \left(n + \frac{1}{2}\right) + \hbar\omega_- \left(m + \frac{1}{2}\right) + \hbar\omega_0 \left(q + \frac{1}{2}\right) \quad \text{Eq.(2.1.10),}$$

where $\omega_{\pm} = \omega_h \pm \frac{1}{2}\omega_c$, $\omega_h = \sqrt{\omega_0^2 + \frac{1}{4}\omega_c^2}$, and $\omega_c \equiv eB/m^*c$ is the cyclotron frequency of the applied magnetic field.

In the following sections, we apply the model to various NCs, ranging from symmetric NCs with/without a magnetic field to asymmetric nanorods without a magnetic field.

a. Absence of a magnetic field

In the absence of a magnetic field, $\omega_+ = \omega_- = \omega_z = \omega_0$, and the energy is simplified to

$$E_{B=0} = \left(\frac{3}{2} + n + m + q\right)\hbar\omega_0. \quad \text{Eq. (2.1.11)}$$

This implies that the energies of all eigenstates with the same states $n + m + q$ are the same.

Each state $(n + m + q)$ corresponds to a degenerate shell. Let us describe some of these shells.

The lowest one, termed the s-shell, consists of only one state $n = m = q = 0$. (Here, we neglect the effect due to spin.) The second one, known as the p-shell, consists of states $|n, m, q\rangle = |1, 0, 0\rangle, |0, 1, 0\rangle,$ and $|0, 0, 1\rangle$. Subsequent states can be generated similarly.

Alternatively, this method can be described by making a linear transformation from the (x, y) basis to the *(clockwise, counterclockwise)* basis just like we can mathematically analyze any linear polarized light beam to a linear combination of two circular polarized ones. Here, the coordinates are a measure of the oscillation amplitudes. Therefore, the quantum numbers n and m differ from n_x and n_y , while $q = n_z$. In fact, either n or m contains information on x and y .

In the figure representing of this method, we can see the energy spectrum versus the z component of angular momentum L_z , as shown in (FIG. 2.1.2). This implies that the energy

eigenstates under this basis are also the eigenstates of \hat{L}_z .

$$\hat{L}_z |n, m, q\rangle = (n - m)\hbar |n, m, q\rangle \quad \text{Eq. (2.1.12),}$$

$$L_z = (n - m)\hbar \quad \text{Eq. (2.1.13).}$$

(However, the energy states in the first method are not the eigenstates of \hat{L}_z , i.e., $\hat{L}_z |n_x, n_y, n_z\rangle \neq L_z |n_x, n_y, n_z\rangle$). In the s-shell, there is only one state, while in the p-shell, there are three states corresponding to different magnetic quantum numbers $M = 1, 0, \text{ and } -1$, these results agree with those of the second method. Thus, for every state in the third method has a “mapping” state in the second method; for example, the state $|N, L, M\rangle = |0, 0, 0\rangle$ in the second corresponds to $|n, m, q\rangle = |0, 0, 0\rangle$ in the third, $|1, 0, 0\rangle$ in the second corresponds to $|1, 1, 1\rangle$ in the third, $|0, 1, 0\rangle$ in the second corresponds to $|1, 1, -1\rangle$ in the third, and $|0, 0, 1\rangle$ in the second corresponds to $|1, 1, 0\rangle$ in the third.

Can we conclude that all the states $|n, m, q\rangle$ in the third approach are the eigenstates of \hat{L}^2 due to the mapping relations shown above? The answer is “No.” The d-shell, has six degenerate states; four of them have different values of L_z , while the other two have $L_z = 0$.

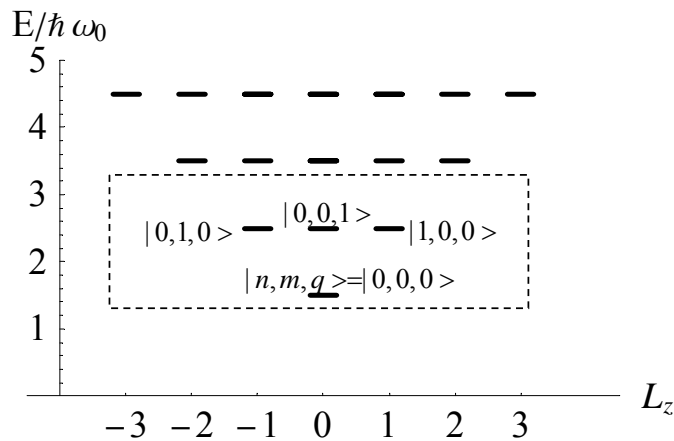


FIG 2.1.2 Energy spectrum versus angular momentum L_z of a single electron subjected to a 3D isotropic parabolic potential with the characteristic confining frequency ω_0 . Each state corresponds to a state one $|n, m, q\rangle$.

Due to the non-degeneracy of L_z , the states $|n, m, q\rangle$ are no longer the eigenstates of \hat{L}^2 .

To obtain the eigenstates of \hat{L}^2 under this condition, we must make a linear combination of all the states $|n, m, q\rangle$, which are in the same shell, with the same L_z . For example, the state

$|N, L, M\rangle = |2, 2, 0\rangle$ corresponds to the superposition of $|n, m, q\rangle = |1, 1, 0\rangle$ and $|0, 0, 2\rangle$,

which can be normalized as $\frac{1}{\sqrt{3}}|1, 1, 0\rangle - \sqrt{\frac{2}{3}}|0, 0, 2\rangle$. Similarly, the representation of state

$|N, L, M\rangle = |2, 0, 0\rangle$ under the basis of the third approach is $\sqrt{\frac{2}{3}}|1, 1, 0\rangle + \frac{1}{\sqrt{3}}|0, 0, 2\rangle$. We

can understand why the states $|n, m, q\rangle$ with the same L_z are not the eigenstates of \hat{L}^2 by

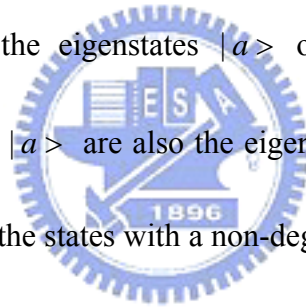
reviewing a theorem in quantum mechanics. The theorem states that if two operators

\hat{A} and \hat{B} commute and the eigenstates $|a\rangle$ of \hat{A} that satisfy $\hat{A}|a\rangle = a|a\rangle$ are

nondegenerate, then the states $|a\rangle$ are also the eigenstates of operator \hat{B} . Thus, since \hat{L}^2

and \hat{L}_z are always commute, the states with a non-degenerate L_z must be the eigenstates of

\hat{L}^2 ; on the other hand, the states with a degenerate L_z are not.



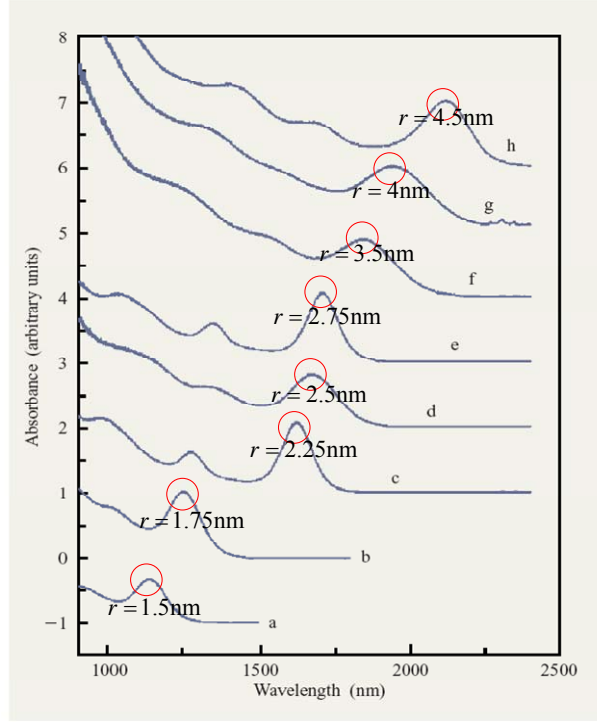


FIG. 2.1.3. Several absorption spectra of PbSe NCs corresponding to various sizes, and the peaks indicate the first optical transition energy.

We compare the data from parabolic model with that from an optical experiment. The transition energy of NCs can be examined optically. FIG. 2.1.3 shows several absorption spectra of PbSe NCs corresponding to various sizes, and the first peak of each spectrum indicates the first transition energy [20]. We can compare these experimental data with the calculation results based on the parabolic model. In the isotropic parabolic model, the ground state energy of a single electron and a single hole can be expressed as

$$E_e = \frac{3}{2} \hbar \omega_e = \frac{3\hbar^2}{4m_e^* l^2}, \quad \text{Eq. (2.1.14a).}$$

$$E_h = \frac{3}{2} \hbar \omega_h = \frac{3\hbar^2}{4m_h^* l^2}, \quad \text{Eq. (2.1.14b).}$$

where ω_e and ω_h are the characteristic frequency of electrons and holes corresponding to their effective masses m_e^* and m_h^* , respectively, and l is the mean motion radius of the particle in NCs which is nearly equal to the actual radius of the system r , i.e.,

$$l \approx r \quad \text{Eq. (2.1.15).}$$

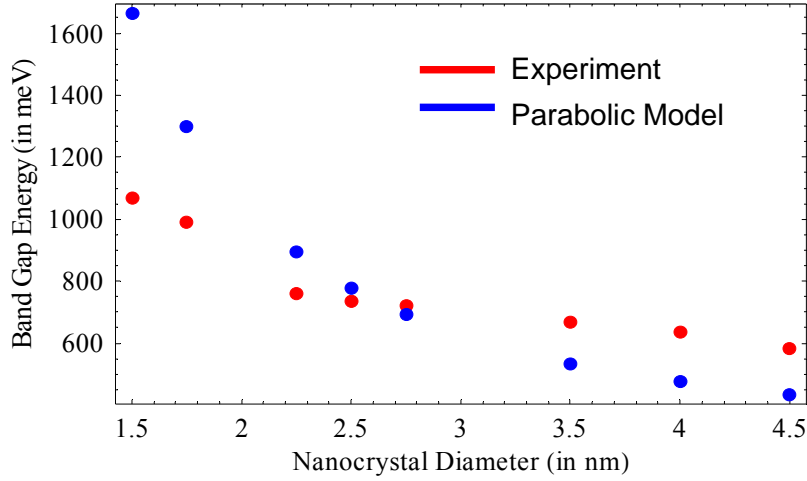


FIG. 2.1.4. Experimental and calculated band gap energy. The trends are similar and thus the parabolic model is suitable to some degree.

Thus, the first transition energy E_t is

$$E_t = E_e + E_h + E_g - V_0. \quad \text{Eq. (2.1.16),}$$

where E_g is the band-gap energy and $E_g = 280$ meV for PbSe; V_0 is the attractive Coulomb energy between the electron and the hole (both of them are in the s-shell). The Coulomb energy is much smaller than other terms so that we ignore it here. Thus the transition energy Eq. (2.1.16) is simplified to

$$E_t \approx E_e - E_h + E_g = \frac{3\hbar^2}{4r^2} \left(\frac{1}{m_e^*} + \frac{1}{m_h^*} \right) + 280(\text{meV}). \quad \text{Eq. (2.1.17)}$$

By considering the effective masses of the electrons and holes in PbSe ($m_e^* = 0.04$ and $m_h^* = 0.034$), we can calculate the transition energy. FIG. 2.1.4 shows the experimental and calculated results. The trends are similar and thus the parabolic model is suitable to some degree.

b. Presence of an external magnetic field

In this section, we consider an NC in the 3D parabolic model with external magnetic fields. The ratio of the characteristic frequency and the cyclotron frequency, ω_c / ω_0 , is frequently

used in this thesis to characterize the field strength in comparison with the strength of the confinement of NCs. The typical value of the original oscillation energy $\hbar\omega_0$ for a nanocrystal system is approximately 100 meV and the corresponding frequency ω_0 is $1.52 \times 10^{14} \text{ s}^{-1}$. If the maximum magnitude of the magnetic field that can be applied is 20 T, then the corresponding maximum value of ω_c is 2.7×10^{13} when the effective mass of CdSe is 0.13, which is the value for a typical semiconductor. Therefore, it is reasonable to set the maximum value of ω_c / ω_0 to 1.

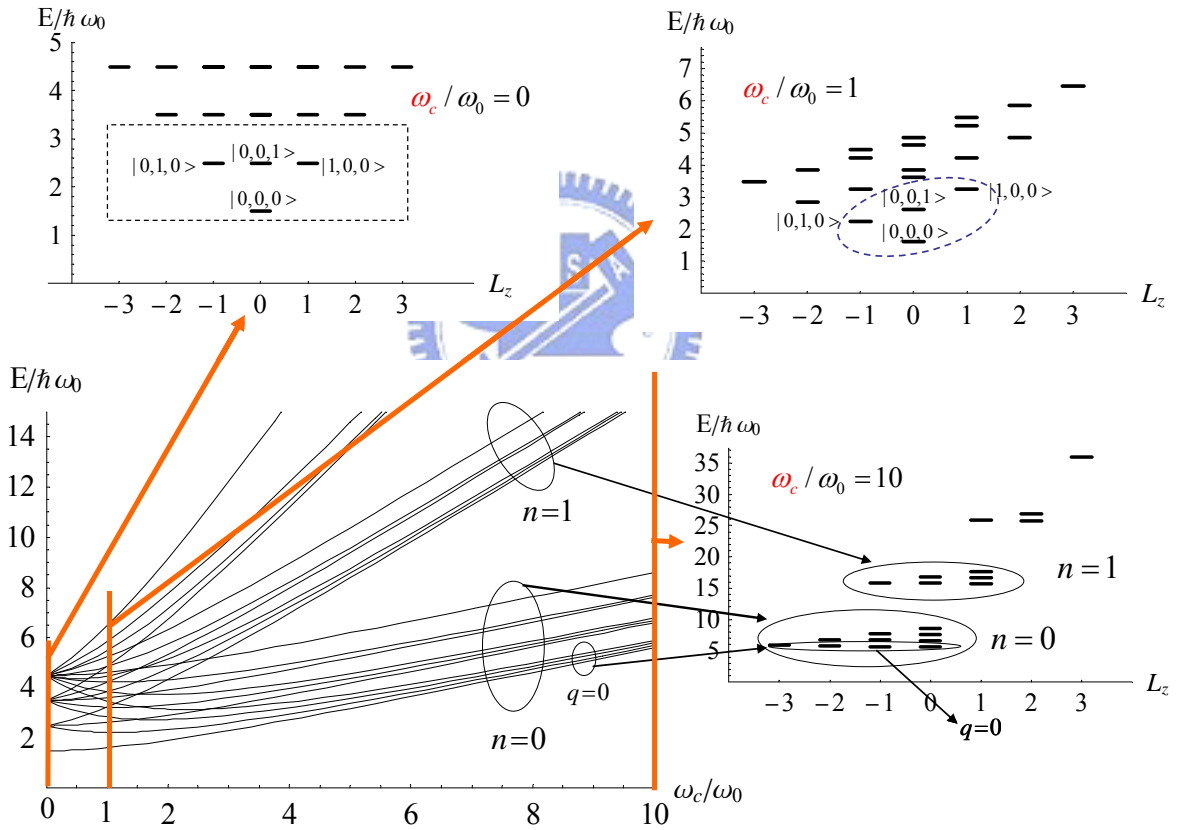


FIG. 2.1.5. Energy spectrum of few lowest states of the single electron in a nanocrystal versus an external magnetic field. The inset shows the reasonable regime wherein the maximum magnetic field is quite feasible. Energy spectrum against L_z when $\omega_c / \omega_0 = 1$ and 10 are also shown.

In FIG. 2.1.5, we show a few low-lying energies as a function of the magnetic field (bottom Left). The energy shift can be explained by the Hamiltonian

$$\begin{aligned}\hat{H} &= \frac{1}{2m^*} \left(\mathbf{p} - \frac{e}{c} \mathbf{A} \right)^2 + \frac{1}{2} m^* \omega_0^2 r^2 \\ &= \frac{p_x^2 + p_y^2}{2m^*} + \frac{1}{2} m^* \omega_h^2 (x^2 + y^2) - \frac{1}{2} \omega_c \hat{L}_z + \frac{p_z^2}{2m^*} + \frac{1}{2} m^* \omega_0^2 z^2.\end{aligned}\tag{Eq.(2.1.18)}$$

The magnetic field effects are contributed by the terms $\frac{1}{2} m^* \omega_h^2 (x^2 + y^2)$ and $-\frac{1}{2} \omega_c \hat{L}_z$; we could state that the former causes the diamagnetic energy shift, while the latter causes the paramagnetic energy shift (Zeeman orbital term). When the magnetic field is small, the linear term dominates and the energy shift is proportional to L_z (the minus sign indicates that the energy reduces and hence we refer to the latter as a “paramagnetic” term) and ω_c . As the magnetic field increases, the diamagnetic (parabolic) term becomes dominant and the energy shift is proportional to ω_h^2 and $x^2 + y^2$. Irrespective of the behavior of the angular momentum the energy increases with the magnetic field and hence the former term is referred to as a “diamagnetic” term.

Readers may find that the energy of state $|1,1,0\rangle$ is higher than that of state $|0,0,2\rangle$, the difference is due to the effect of the diamagnetic term since both the states have the same L_z .

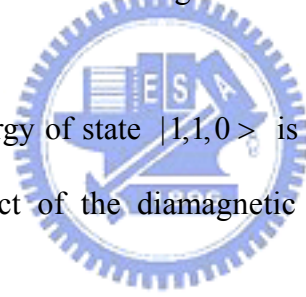


FIG. 2.1.3 also shows how the system evolves as the magnetic field increases significantly since interesting physics has been observed in SAQD systems. As $\omega_c \gg \omega_0$,

$$\begin{aligned}E &= \hbar \omega_+ \left(n + \frac{1}{2} \right) + \hbar \omega_- \left(m + \frac{1}{2} \right) + \hbar \omega_0 \left(q + \frac{1}{2} \right) \\ &\approx \hbar \omega_c \left(n + \frac{1}{2} \right) + \hbar \omega_0 \left(q + \frac{1}{2} \right) \\ &\approx \hbar \omega_c \left(n + \frac{1}{2} \right).\end{aligned}\tag{Eq.(2.1.19)}$$

Therefore, the energy states are asymptotic to the Landau levels and are dominated by the quantum number n as the magnetic field is considerably large.

On the right hand side of FIG. 2.1.3, we can find four Landau levels corresponding to different values of n , and each level is split into some sublevels due to different original

oscillation energies in the z direction (which correspond to different values of q). If we observe more carefully, we can find that there are still splitting levels due to different values of m . Thus, if we consider a larger number of shells, all the lowest energy states in the large field limit would be $|0, m, 0\rangle$, where m ranges from 0 to an arbitrary large number. To understand this concept further, let us consider a classical picture. When a charged particle is moving in a 2D system under the influence of a magnetic field, the particle rotates circularly due to the Lorenz force; the frequency of the particle rotation is $\omega_c = qB/m$, where q is the charge of the particle, m is its mass, and B is the applied magnetic field. Both

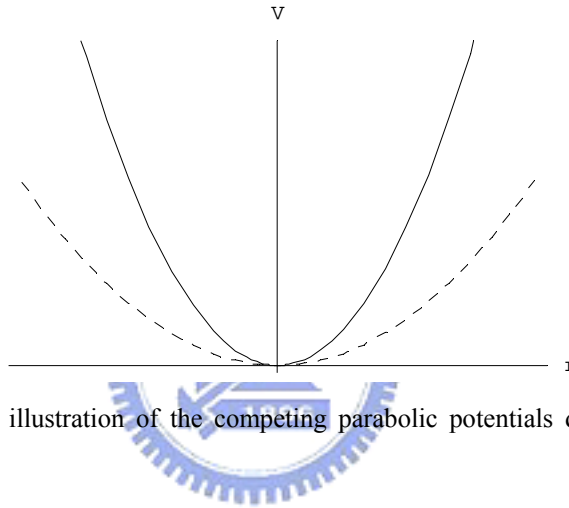


FIG. 2.1.6 A graphical illustration of the competing parabolic potentials due to the system and the magnetic field.

the radius of the motion circle and the energy of the particle are continuous. In the quantum mechanical picture, however, the energy is not continuous but splits into an energy level $E_c = (n + \frac{1}{2})\hbar\omega_c$, which is known as the Landau level, where \hbar is the Planck constant and n is a definite positive integer. Since the circular motion can be considered a 2D SHO, we may treat the charged particle under a magnetic field as a particle in a 2D parabolic potential. Thus if we place a charged particle in a 2D parabolic potential and apply a magnetic field normal to the 2D plane, it can be equivalently considered that there are two SHOs that compete to the dominate the motion. FIG. 1.4 provides a graphical illustration of the competing parabolic potential due to the system and the magnetic field. When the magnetic

field is sufficiently strong (solid line), the magnetic Landau term is dominant; however, when the field is weak (dashed line), the original SHO is dominant.

2.2 3D Anisotropic Parabolic Model

In this section, we investigate the effect of anisotropy on the single electron spectrum of elongated NCs/NRs. The elongation of the geometry NRs is characterized by the ratio ω_0 / ω_z or l_z / l_0 , where ω_0 and ω_z are the characteristic frequencies in the x-y plane and along the z-axis, respectively; l_0 and l_z are the confining lengths in the xy-plane and along the z-axis, which are defined as $l_{0(z)} = \sqrt{\hbar / 2m\omega_{0(z)}}$ in previous sections. Here we focus only on the system elongated in the z-direction, i.e., $l_x = l_y \neq l_z$, to address the subject of the NR system later. In fact, we find that the effect of the elongation on the electronic structure is analogous to the effect of applying a magnetic field. This allows us to consider shape control to replace external fields for the engineering of the electronic structure of NCs. The Hamiltonian of the anisotropic parabolic system is written as

$$\hat{H} = \frac{\mathbf{p}^2}{2m^*} + \frac{1}{2} m^* (\omega_0^2 x^2 + \omega_0^2 y^2 + \omega_z^2 z^2) \quad \text{Eq.(2.2.1)}$$

Since there is no applied magnetic field and the system is anisotropic in z-direction,

$$\omega_+ = \omega_- = \omega_0,$$

$$\omega_z \neq \omega_0;$$

then the energy becomes

$$E = \hbar\omega_0(n+m+1) + \hbar\omega_z\left(q + \frac{1}{2}\right) \quad \text{Eq.(2.2.2).}$$

FIG. 2.2.1 shows a plot of the energy spectrum against the magnitude of anisotropy (bottom left), which is represented by the aspect ratio l_z / l_0 . The expression $\omega_0 / \omega_z = 4$ indicates that the confining length in the direction of the z-axis is twice the length on the xy-plane, i.e.,

$$\omega_0 / \omega_z = 4 \Rightarrow l_z = 2l_x = 2l_y.$$

There are two limiting conditions in this specific system. At the extreme left of the plot, the ratio ω_0/ω_z is 1, which implies that the system is isotropic and the energy is dominated by the 3D shell structure. The spectrum and the degeneracy in this condition have been discussed in Chapter 2.1. At the extreme right of all the plot, all the states $|n,m,q\rangle$ with fixed values of n and m fall toward an asymptotic state $|n,m,0\rangle$. However, they could never “arrive” there because our system is still a 3D system. Thus when the ratio ω_0/ω_z increases substantially, the lowest states are the states $|0,0,q\rangle$, where q is from 0 to any arbitrary large number. The quantization is caused by the different oscillation amplitudes, and when

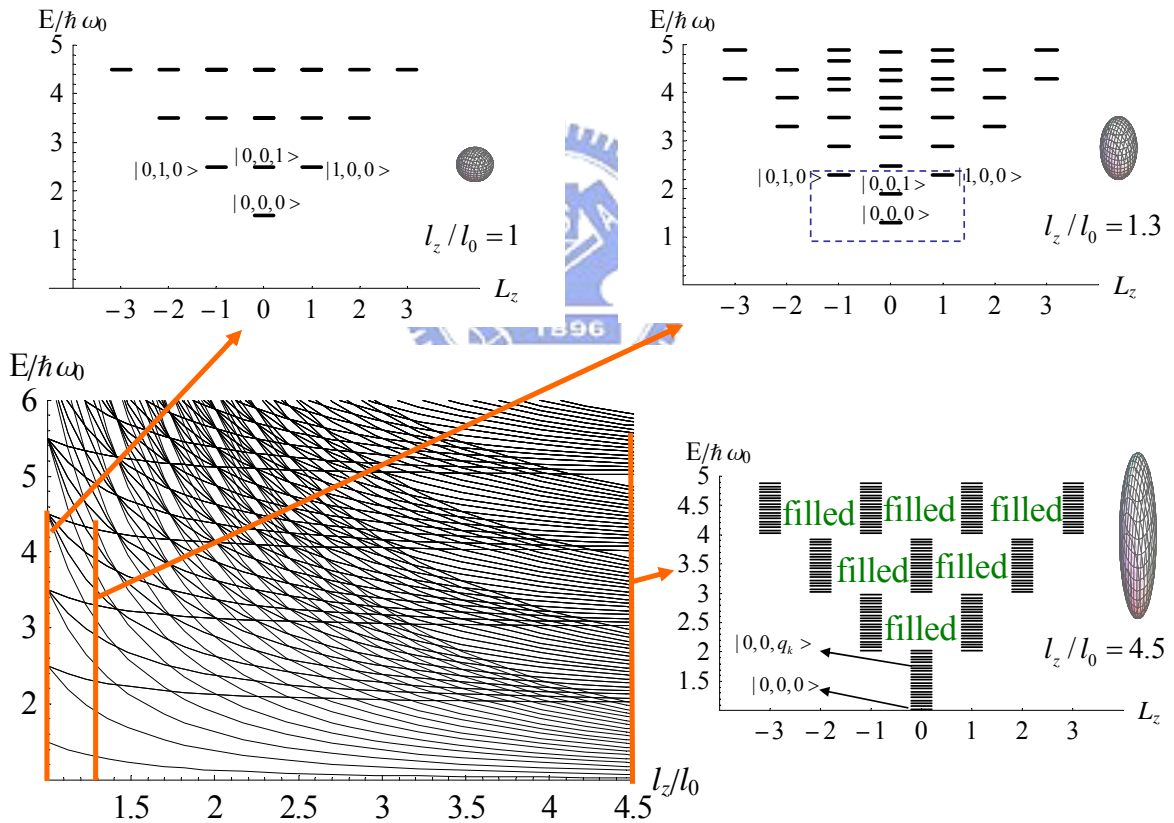


FIG. 2.2.1 Energy spectrum of the lowest shells of an elongated NC versus aspect ratio l_z/l_0 . Plots of the energy spectrum against L_z when $l_z/l_0 = 1, 1.3,$ and 4.5 are also shown. Note that when the aspect ratio increases, the difference between the lowest energy states decreases significantly such that they resemble continuous states.

ω_0/ω_z goes to infinity, the states could be approximated as quasi-continuous states.

FIG. 2.2.1 (bottom right) shows the quasi-continuous states. The figure is limited to 20 shells, hence the states at the right limit resemble “belts.” If we consider a large number of shells, the right limit states will be similar to continuous states, i.e., an energy “band.” FIG. 2.2.1 (bottom right) clearly shows that the lowest states are $|0,0,0\rangle$, $|0,0,1\rangle$, $|0,0,2\rangle$

In the mediate condition, all the state energies lower as the system is elongated. Let us observe some of the lowest states here. In the s-shell the energy of state $|0,0,0\rangle$ is $E/\hbar\omega_0 = 1 + \frac{1}{2\omega_0/\omega_z}$, which decays as ω_0/ω_z increases. In the p-shell both the states $|1,0,0\rangle$ and $|0,1,0\rangle$ have the energy $E/\hbar\omega_0 = 2 + \frac{1}{2\omega_0/\omega_z}$ and are degenerate, while state $|0,0,1\rangle$ decays more rapidly because its energy is $E/\hbar\omega_0 = 1 + \frac{3}{2\omega_0/\omega_z}$.

On the other hand, when the system is compressed, all the states with $q \neq 0$ are raised and the lowest states are essentially the Fock-Darwin states in the 2D cases. In FIG. 2.2.3 we show the energy spectrum with $l_z/l_0 = 0.5$. It should be noted that the states are essentially the Fock-Darwin states.

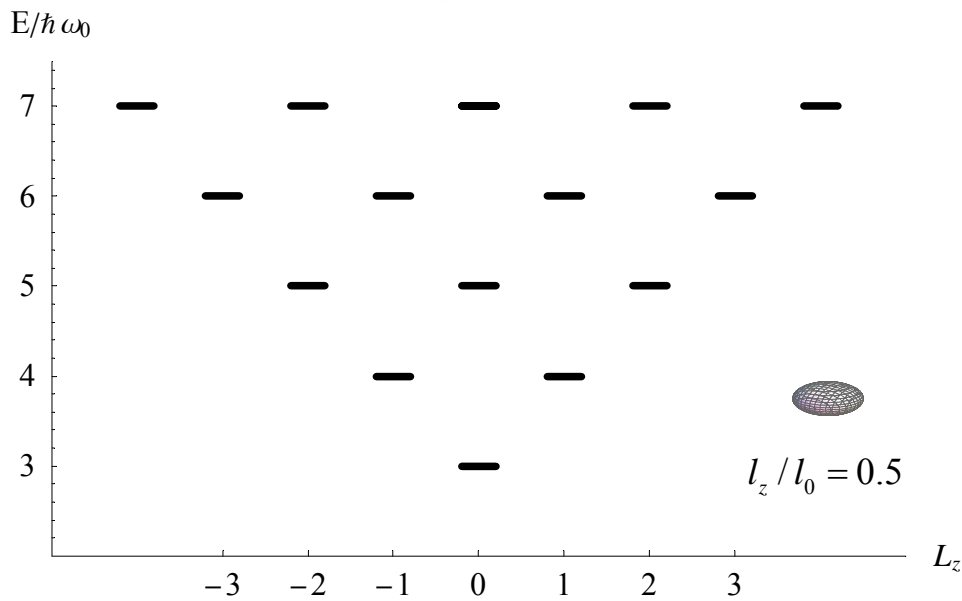


FIG. 2.2.2 Energy spectrum versus L_z as ω_0/ω_z tends to infinity. The spectrum with a low value of anisotropy ($\omega_z > \omega_0$) approaches the Fock-Darwin spectrum of a 2D parabolic system.

Chapter 3: Configuration Interaction Theory for Nanocrystal/Nanorods

In this chapter, we describe the configuration interaction (CI) theory for the few-electron problem of 3D confinement nanostructures. For studies of interacting electrons in NC/NR systems, we develop the CI theory for the calculation of the spectrum of few electrons subjected to an isotropic and/or anisotropic parabolic potential with or without magnetic fields. We derive the explicit formulation of the Coulomb matrix elements that are required in the theory and conducted the evaluations in a simple semi-analytical manner.

The full Hamiltonian for many interacting electrons in an NC is expressed in terms of the second quantization as

$$H = \sum_i E_i c_i^\dagger c_i + \frac{1}{2} \sum_{ijkl} \langle ij | V | kl \rangle c_i^\dagger c_j^\dagger c_k c_l, \quad \text{Eq.(3.1)}$$

where $i, j, k,$ and l represent the quantum number $n, m,$ and q of the two interacting electrons before and after the interaction, i.e.,

$$i = (n_1', m_1', q_1'),$$

$$j = (n_2', m_2', q_2'),$$

$$k = (n_2, m_2, q_2),$$

$$l = (n_1, m_1, q_1);$$

E_i is the kinetic energy mentioned in Chapter 2,

$$E_i = \hbar\omega_+(n_i + \frac{1}{2}) + \hbar\omega_-(m_i + \frac{1}{2}) + \hbar\omega_z(q_i + \frac{1}{2}), \quad \text{Eq.(3.2)}$$

$\langle ij | V | kl \rangle$ is the Coulomb interaction energy, and c_i^\dagger 's and c_i 's are the creation and annihilation operators of electrons with quantum numbers $n, m,$ and q . The single electron

kinetic energy is essentially the eigenenergy of the single electron Hamiltonian described in Ch. 2. The coulomb matrix element in the basis of the single electron state is formulated by evaluating a 6-dimensional integral (See Appendix for a detailed derivation).

$$\begin{aligned}
\langle ij | V | kl \rangle = & \frac{1}{l_z} \times \frac{\delta_{R_L, R_R} \cdot \delta_{q_1'+q_1+q_2'+q_2, \text{even}} \cdot (-1)^{n_2'+m_2'+q_2'+n_2+m_2+q_2}}{\pi \sqrt{n_1! m_1! q_1! n_1! m_1! q_1! n_2! m_2! q_2! n_2! m_2! q_2!}} \\
& \times \sum_{p_1=0}^{\min(n_1', n_1)} \sum_{p_2=0}^{\min(m_1', m_1)} \sum_{p_3=0}^{\min(q_1', q_1)} \sum_{p_4=0}^{\min(n_2', n_2)} \sum_{p_5=0}^{\min(m_2', m_2)} \sum_{p_6=0}^{\min(q_2', q_2)} \{p_1! p_2! p_3! p_4! p_5! p_6! \\
& \times \binom{n_1'}{p_1} \binom{n_1}{p_1} \binom{m_1'}{p_2} \binom{m_1}{p_2} \binom{q_1'}{p_3} \binom{q_1}{p_3} \binom{n_2'}{p_4} \binom{n_2}{p_4} \binom{m_2'}{p_5} \binom{m_2}{p_5} \binom{q_2'}{p_6} \binom{q_2}{p_6} \\
& \times (-1)^{u+v} \times \left(\frac{\omega_z}{2\omega_h} \right)^u \\
& \times \frac{\Gamma(1+u)\Gamma(\frac{1}{2}+v)\Gamma(\frac{1}{2}+u+v)}{\Gamma(\frac{3}{2}+u+v)} \times {}_2F_1 \left(1+u, \frac{1}{2}+u+v; \frac{3}{2}+u+v; 1 - \frac{\omega_z}{\omega_h} \right) \quad \text{Eq. (3.3)}
\end{aligned}$$

Eq. (3.3) shows a generalized formulation of the Coulomb matrix elements (in effective Rydberg unit) for arbitrary SHO systems with/without a magnetic field, where $l_0 = \sqrt{\hbar/2m\omega_0}$ is the characteristic confining length of the system,

$$u = m_1' + m_2' + n_1 + n_2 - (p_1 + p_2 + p_4 + p_5),$$

$$v = \frac{q_1' + q_1 + q_2' + q_2}{2} - (p_3 + p_6), \quad {}_2F_1 \text{ is the hypergeometric function, and } x = \omega_z / \omega_h. \text{ The}$$

elements can be evaluated in a simple semi-analytical or numerical fashion. In the following analysis, we show the relevant matrix elements for the two lowest electronic shells of NCs in magnetic fields.

To calculate the energy spectrum of a few interacting electrons in an NC, we first develop the few-electron configurations and classify the configurations of the conserved variables of the system, e.g., the total spin, z-component of the total spin, and z-component of the total angular momentum for the systems considered in this thesis. This classification of the configuration divides the Hilbert space into several decoupled subspaces and helps us to

reduce the dimension of the Hamiltonian matrix that requires diagonalization. Finally, we

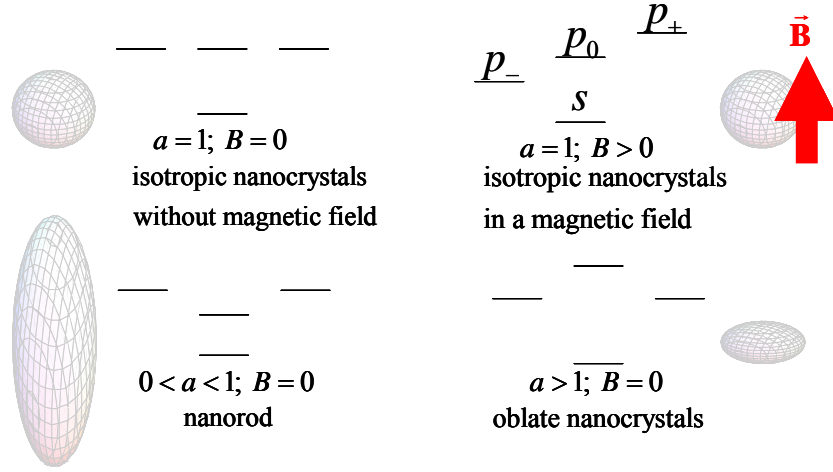


FIG. 3.1 Two-shell structures examined in this chapter. Here, $a \equiv l_z / l_0$ is the aspect ratio and B is the applied magnetic field.

determine the eigenenergies and eigenstates of the system via direct diagonalization. FIG. 3.1 shows the shell structures of the NCs under consideration, on which few-electron configurations will be constructed.

For simplicity, we use the two-shell approximation in our calculation (in principle, we should consider an infinite number of shells to obtain accurate results). Due to spin, each orbital is doubly degenerate. Thus in a two-shell case, there are eight states that could be occupied. For convenience, the 4 orbitals are labeled s , p_- , p_0 , and p_+ (top right of FIG. 3.0.1). Therefore, there are $C_2^8 = 28$ possible configurations in total. We show the total 28 configurations in FIG. 3. 2. The configurations are grouped by the total spin (singlet or triplet) and the z-component of the total angular momentum. Additionally, we denote the terms in the configuration as $|s01\rangle$, $|s02\rangle$,... and $|t01\rangle$, $|t02\rangle$..., where s and t denote the singlet and triplet states, respectively.

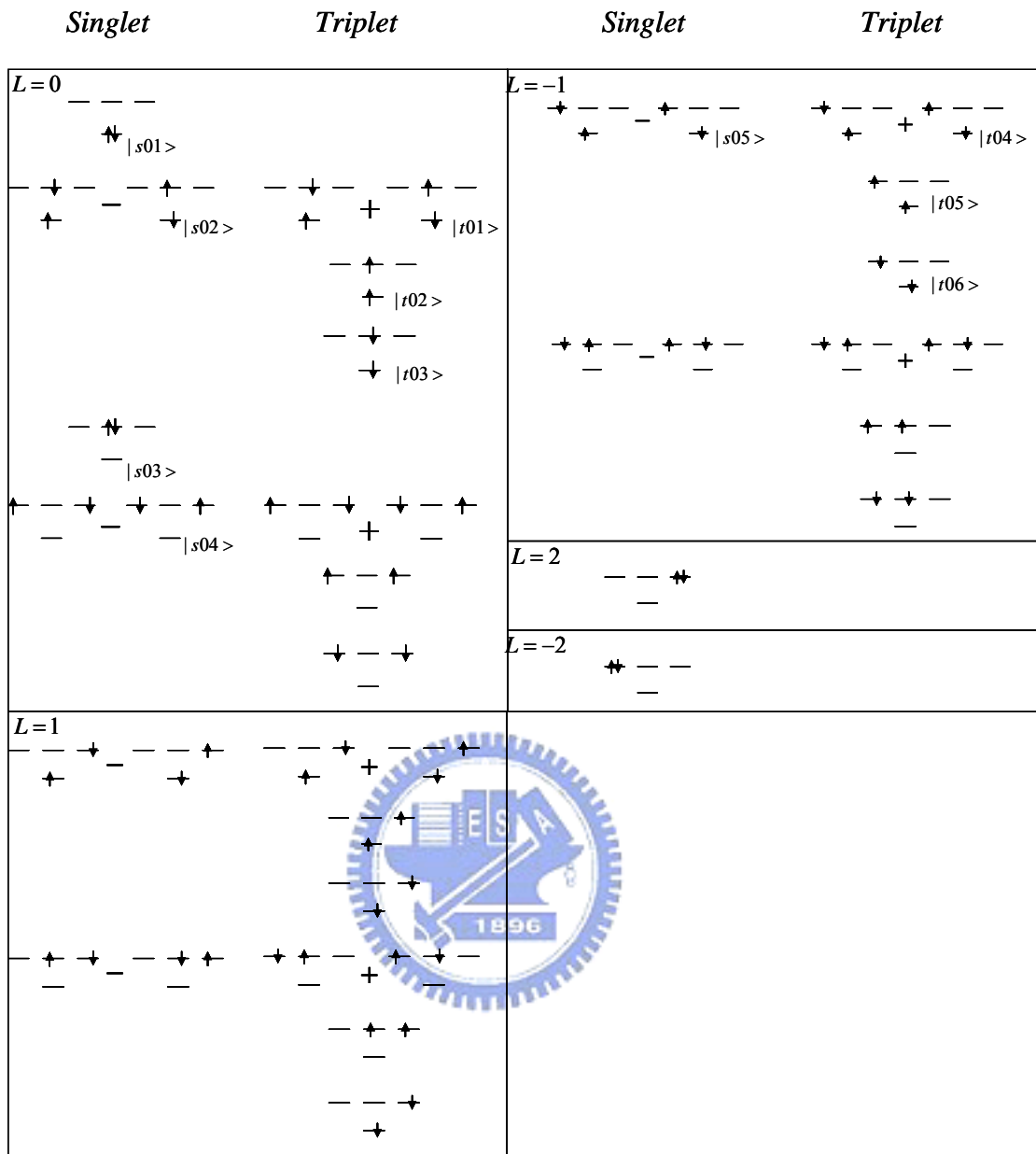


FIG. 3.2 The 28 configurations in the 2-shell approximation. The configurations are classified by the total spin and the z-component of the total angular momentum. The configurations that are of concern are labeled.

Chapter 4: Results

In this chapter, we apply the theory described in chapter 3 to three simple representative cases, i.e. two mutually interacting electrons in (1) two mutually interacting electrons in an isotropic nanocrystal without a magnetic field, (2) two mutually interacting electrons in an isotropic nanocrystal under an external magnetic field, and (3) two mutually interacting electrons in an anisotropic NC (NR). We calculate the ground states and the energy spectrum of the two electron systems using the partial CI approach within the simple two-shell approximation and explore the possibility of the singlet/triplet (S/T) state transitions, a physical phenomenon that is the manifestation of particle-particle interaction in QDs, driven by magnetic fields and/or deformation of NCs.



4.1. Two Electrons in an Isotropic Nanocrystal without Magnetic Field

In the basis of the three lowest kinetic energy configurations listed in FIG. 3.2 $|s01\rangle$, $|s03\rangle$ and $|s04\rangle$ (due to the parity, $|s02\rangle$ does not couple with them.), the Hamiltonian of two interacting electrons in a spherical nanocrystal at $B = 0$ is given by

$$H = \begin{pmatrix} \langle s01 | H | s01 \rangle & \langle s01 | H | s03 \rangle & \langle s01 | H | s04 \rangle \\ \langle s03 | H | s01 \rangle & \langle s03 | H | s03 \rangle & \langle s03 | H | s04 \rangle \\ \langle s04 | H | s01 \rangle & \langle s04 | H | s03 \rangle & \langle s04 | H | s04 \rangle \end{pmatrix} \quad \text{Eq. (4.1.1).}$$

The configurations can be represented as $|s01\rangle = c_{000,\downarrow}^+ c_{000,\uparrow}^+ |vac\rangle$, $|s03\rangle = c_{001,\downarrow}^+ c_{001,\uparrow}^+ |vac\rangle$,

and $|s04\rangle = \frac{1}{\sqrt{2}}(c_{010,\downarrow}^+ c_{100,\uparrow}^+ |vac\rangle - c_{010,\uparrow}^+ c_{100,\downarrow}^+ |vac\rangle)$, where $|vac\rangle$ is the vacuum state.

Now we calculate the matrix elements. Considering $|s01\rangle$ and the configurations in the Hamiltonian Eq. (3.1), we have

$$\begin{aligned}
& \langle s01 | H | s01 \rangle = \langle vac | c_{000,\uparrow} c_{000,\downarrow} H c_{000,\downarrow}^+ c_{000,\uparrow}^+ | vac \rangle \\
& = E(0,0,0) + E(0,0,0) + \frac{1}{2} (\langle 000;000 | V | 000;000 \rangle + \langle 000;000 | V | 000;000 \rangle) \\
& = 2 \times \left(\hbar\omega_+ \left(0 + \frac{1}{2} \right) + \hbar\omega_- \left(0 + \frac{1}{2} \right) + \hbar\omega_z \left(0 + \frac{1}{2} \right) \right) + \langle 000;000 | V | 000;000 \rangle \\
& = \hbar\omega_+ + \hbar\omega_- + \hbar\omega_z + \langle 000;000 | V | 000;000 \rangle
\end{aligned} \tag{4.1.2}.$$

The calculation involving c_i and c_i^+ obeys the anti-commutation relations

$$\begin{aligned}
& [c_i^+, c_j^+]_+ = c_i^+ c_j^+ + c_j^+ c_i^+ = 0 \\
& [c_i, c_j]_+ = 0 \\
& [c_i, c_j^+]_+ = \delta_{ij}.
\end{aligned} \tag{4.1.3}.$$

Similarly, we have

$$\begin{aligned}
& \langle s01 | H | s03 \rangle = \langle vac | c_{000,\uparrow} c_{000,\downarrow} H c_{001,\downarrow}^+ c_{001,\uparrow}^+ | vac \rangle \\
& = 0 + 0 + \frac{1}{2} (\langle 000;000 | V | 001;001 \rangle + \langle 000;000 | V | 001;001 \rangle) \\
& = \langle 000;000 | V | 001;001 \rangle
\end{aligned} \tag{4.1.4},$$

$$\begin{aligned}
& \langle s01 | H | s04 \rangle \\
& = \frac{1}{\sqrt{2}} (\langle vac | c_{000,\uparrow} c_{000,\downarrow} H c_{100,\downarrow}^+ c_{010,\uparrow}^+ | vac \rangle - \langle vac | c_{000,\uparrow} c_{000,\downarrow} H c_{010,\downarrow}^+ c_{100,\uparrow}^+ | vac \rangle) \\
& = \sqrt{2} \langle 000;000 | V | 100;010 \rangle
\end{aligned} \tag{4.1.5}.$$

$$\begin{aligned}
& \langle s03 | H | s03 \rangle \\
& = \hbar\omega_+ + \hbar\omega_- + 3\hbar\omega_z + \langle 001;001 | V | 001;001 \rangle
\end{aligned} \tag{4.1.6},$$

$$\begin{aligned}
& \langle s03 | H | s04 \rangle = \\
& = \sqrt{2} \langle 001;001 | V | 100;010 \rangle
\end{aligned} \tag{4.1.7},$$

$$\begin{aligned}
& \langle s04 | H | s04 \rangle \\
& = 2\hbar\omega_+ + 2\hbar\omega_- + \hbar\omega_z + \langle 100;010 | H | 100;010 \rangle - \langle 100;010 | H | 100;010 \rangle
\end{aligned} \tag{4.1.8}$$

For the system under consideration in which two interacting electrons are in a spherical nanocrystal at $B = 0$, we have $\omega_+ = \omega_- = \omega_z = \omega_0$. We write

$\langle 000;000 | V | 000;000 \rangle_{B=0} \equiv V_0$ and represent other Coulomb elements in the unit of V_0 .

Some values of some $\langle ij | V | kl \rangle$ are listed in Table 3 in terms of V_0 .

$\langle 000;000 V 000;000 \rangle$	V_0
$\langle 000;000 V 001;001 \rangle$	$\frac{1}{6}V_0$
$\langle 000;000 V 100;010 \rangle$	$\frac{1}{6}V_0$
$\langle 001;001 V 001;001 \rangle$	$\frac{49}{60}V_0$
$\langle 001;001 V 100;010 \rangle$	$\frac{1}{20}V_0$
$\langle 100;010 V 010;100 \rangle$	$\frac{23}{30}V_0$
$\langle 100;010 H 100;010 \rangle$	$\frac{1}{10}V_0$

Table 3. Some values of $\langle ij | V | kl \rangle$ in terms of V_0 under no external magnetic field.

Thus the Hamiltonian can be simplified as

$$H_0 = \begin{pmatrix} 3\hbar\omega_0 + V_0 & \frac{1}{6}V_0 & \frac{\sqrt{2}}{6}V_0 \\ \frac{1}{6}V_0 & 5\hbar\omega_0 + \frac{49}{60}V_0 & \frac{\sqrt{2}}{20}V_0 \\ \frac{\sqrt{2}}{6}V_0 & \frac{\sqrt{2}}{20}V_0 & 5\hbar\omega_0 + \frac{13}{15}V_0 \end{pmatrix} \quad \text{Eq.(4.1.9)}$$

For nanocrystals, the typical value of the ratio of V_0 to ω_0 is small and it is given by

$$V_0 \approx \frac{1}{10}\hbar\omega_0.$$

By diagonalizing the matrix, we obtain the ground state energy given by

$E_{GS} = 3.0996\hbar\omega_0$, which is slightly lower than the value $\langle s01 | H | s01 \rangle = 3.1\hbar\omega_0$ obtained without considering higher shells because of the very strong confinement of the NC and the relatively weak Coulomb interaction strength (small value of $V_0/\hbar\omega_0$). FIG. 3.1.1 shows a plot of the state energy versus the number of configurations considered in the calculation. We

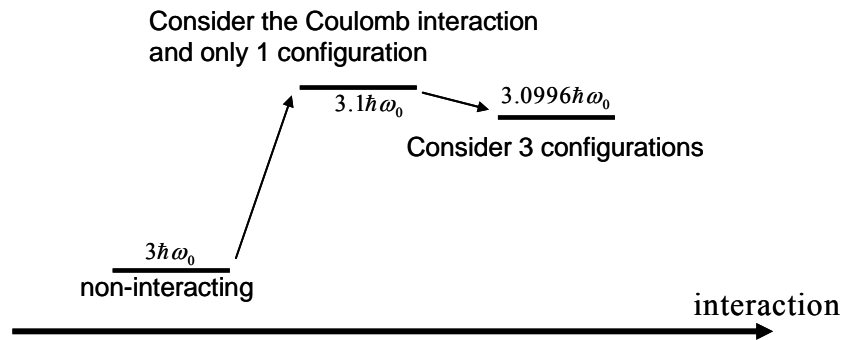


FIG. 4.1.1 Plot of the state energy versus the number of configuration we take into calculation. We could predict that as we take a larger number of basis, the result obtained can be more correct.

could predict that the result obtained here can be more accurate if we use a larger size of basis, the result obtained can be more correct.

4.2. Two Electrons in an Isotropic Nanocrystal in Magnetic Fields

As described in chapter 1, the electronic structure of nanostructure systems can be tuned by an external magnetic field and we are now attempting to examine the effect of magnetic field on the nanocrystal systems. Let us now turn to the case of two electrons in an isotropic nanocrystal in an external magnetic field. In these cases both the kinetic and Coulomb interaction terms in the Hamiltonian matrix elements vary with the magnetic field and become more complicated. Here we solve the 2-electron problem numerically by using a loop to diagonalize the Hamiltonian matrix, as in the previous section, with a slightly varied magnetic field.

The energy spectrum for the 28 configurations of 2 electrons in a spherical nanocrystal and an external magnetic field are shown in FIG. 4.2.1 and FIG. 4.2.2. The three branches in the p-shell (correspond to p_+ , p_0 , and p_- in FIG. 3.1) caused by the Zeeman orbital effect can be seen in both the figures. However, the Coulomb interaction is not considered in FIG. 4.2.1, while FIG. 4.2.2 includes the interaction terms.

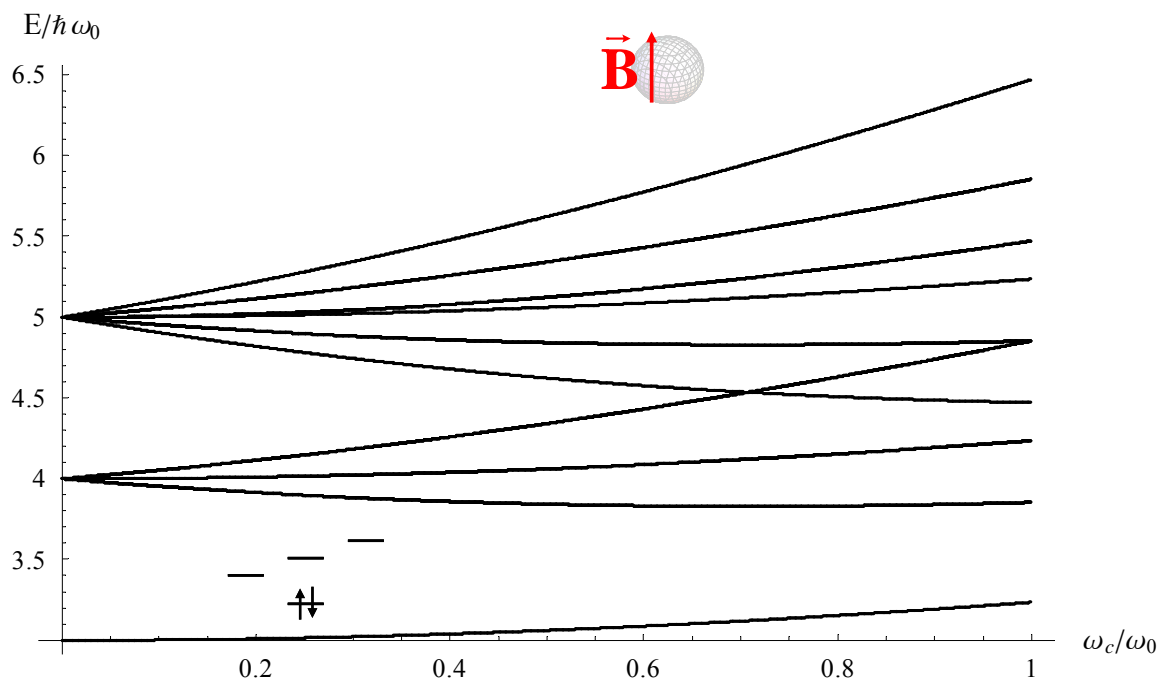


FIG. 4.2.1 2-electron energy spectrum in a spherical nanocrystal versus applied magnetic field in the 2-shell approximation when the interaction terms are ignored. The splittings in the p-shell are caused by the orbital Zeeman effect.

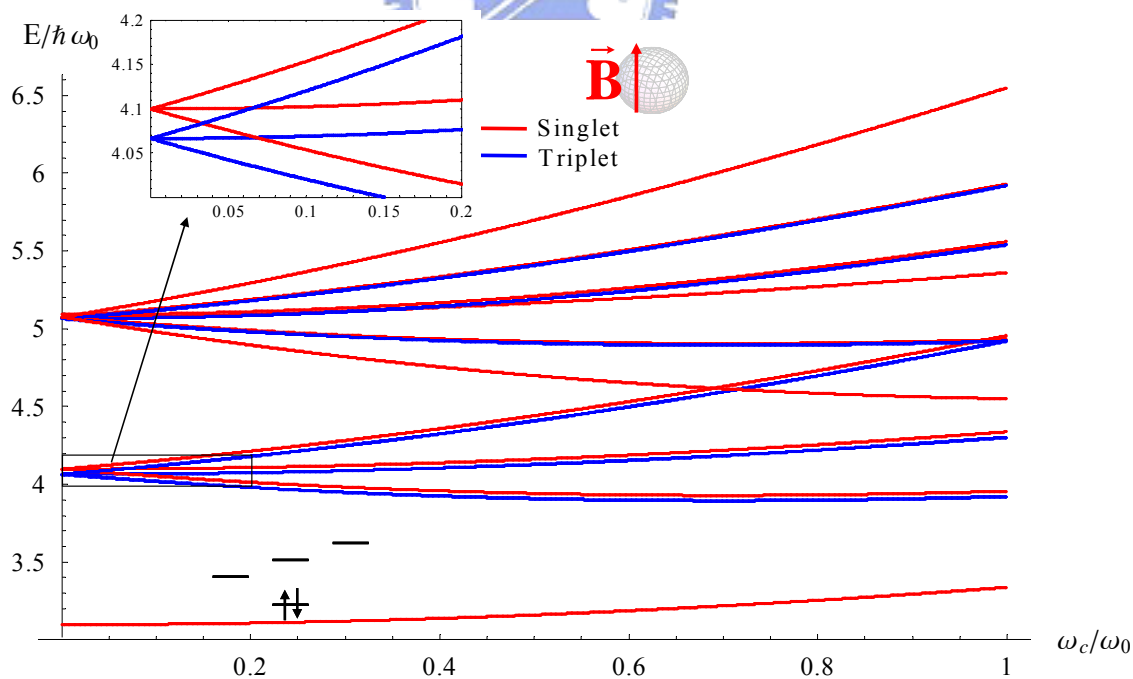


FIG. 4.2.2 2-electron energy spectrum in a spherical nanocrystal versus applied magnetic field in the 2-shell approximation when the interaction terms are included. The hyperfine splittings can be explained by spin exchange terms.

We observe that some states split when the Coulomb interaction is considered. The splittings can be explained by the exchanged energy because the singlet states gain an exchange energy term, while the triplet states lose on one.

FIG. 4.2.3 gives a comparison of the evolution of state energies for three different amplitudes of the magnetic field when the interaction terms are either ignored or included. We observe that the interaction consistently increases the state energy because of the Coulomb repulsive energy. The splittings due to the exchanged energy are not very evident but still observable. It should be noted that the exchange terms split the states and the single-particle spectrum changes the order of states. From FIG. 4.2.3 we see that the electronic structure can be tuned by the external magnetic field due to the inclusion of the interaction energy.

The energy of the orbital p_- (see FIG. 3.1) has been lowered due to the magnetic field and becomes closer to the energy of s orbital. Thus the electrons in the s -shell could have an opportunity to “jump” to the p_- orbital. If an electron jumps to the p_- orbital, the

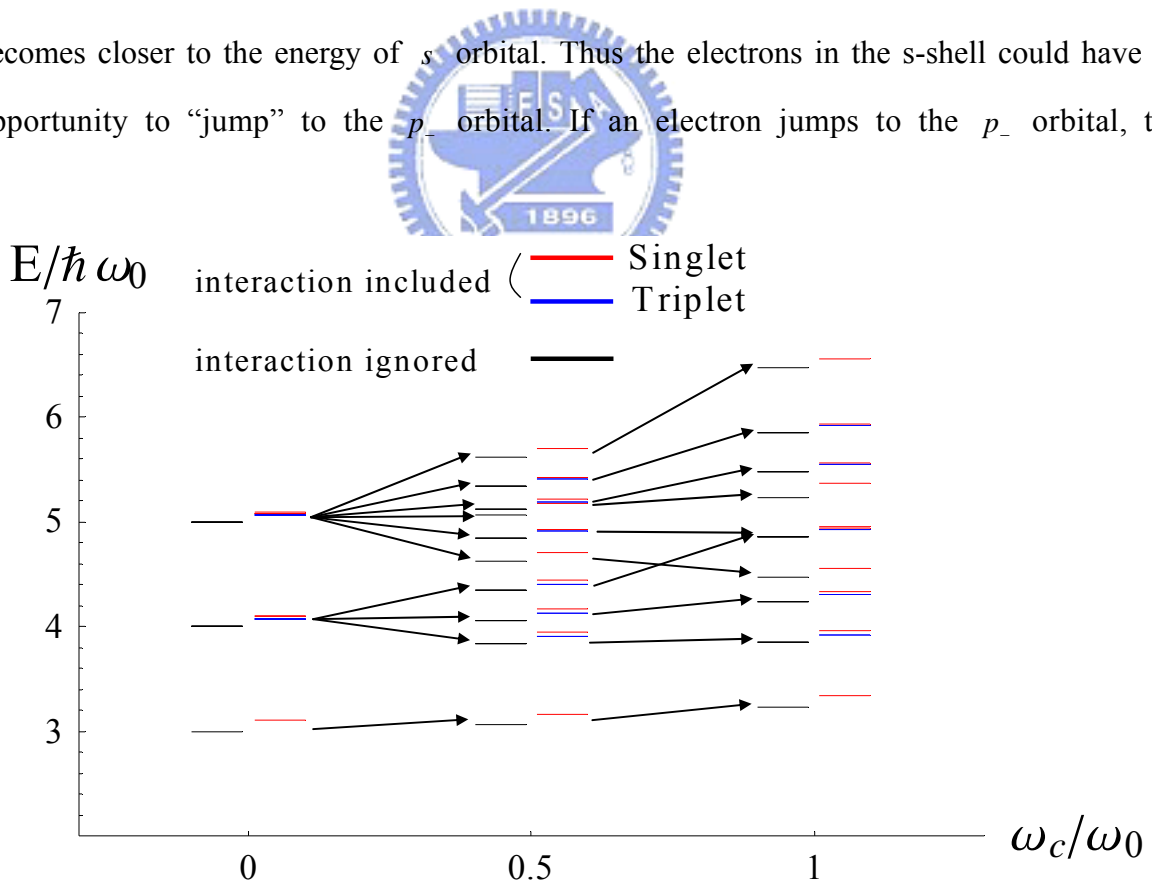


FIG. 4.2.3 Comparison of the evolution of state energies in three different amplitudes of the magnetic field in the condition that the interaction terms are ignored or included. We see that the interaction always make the state energy higher because of the Coulomb repulsive energy. The splittings due to exchange energy are not so obvious but observable.

spin-singlet-triplet transition occurs, just as observed in 2D systems. We can observe a reduction in the energy difference between the singlet and triplet states with a corresponding increase in the magnetic field.

However, there was no crossover in the feasible magnitude of the magnetic field. This is because the size of the system is too small. In a 3D nanocrystal, the Coulomb potential V_0 is smaller than that in a 2D gate-defined QD, while the kinetic energy $\hbar\omega_0$ in a NC is larger than that in a gate-defined QD. Moreover the magnetic length is larger than the confining length of the system. If we intend to observe the crossing in an NC system, we have to increase the magnetic field to an impractical magnitude in the order of 10^0 , which corresponds to few hundreds of Tesla. Although there is no singlet-triplet transition in the ground state, we can still control the electronic structure by applied magnetic field. For example, the lowest 7 states at $\omega_c/\omega_0=0$ are ordered (from low to high) singlet, triplet, triplet, triplet, singlet, singlet and singlet; however, at $\omega_c/\omega_0=0.5$, the order is changed to singlet, triplet, singlet, triplet, singlet, triplet and singlet. The order is changed again if the system is at $\omega_c/\omega_0=1$ (FIG. 4.2.3). These various orders may affect the optical properties and could be used.

4.3. Two Electrons in an Anisotropic System (Nanorod)

Since the shape of nanocrystals can be controlled effectively, we can tune the electronic structure of a nanocrystal by controlling its shape rather than applying a magnetic field. As shown in FIG. 3.1, the shell structure is changed due to the anisotropy, and thus the energy spectrum is also changed. Similar to our method in the previous section, we calculated the eigenenergy numerically by varying the aspect ratio.

The energy spectra of all the configurations are shown in FIG. 4.3.1 and FIG. 4.3.2 where the interaction terms are ignored/included. Note that the elongation of the system (from oblate to

prelate) makes the state energies decay very rapidly such that the energy difference between singlet and triplet states in FIG. 4.3.2 is not very obvious.

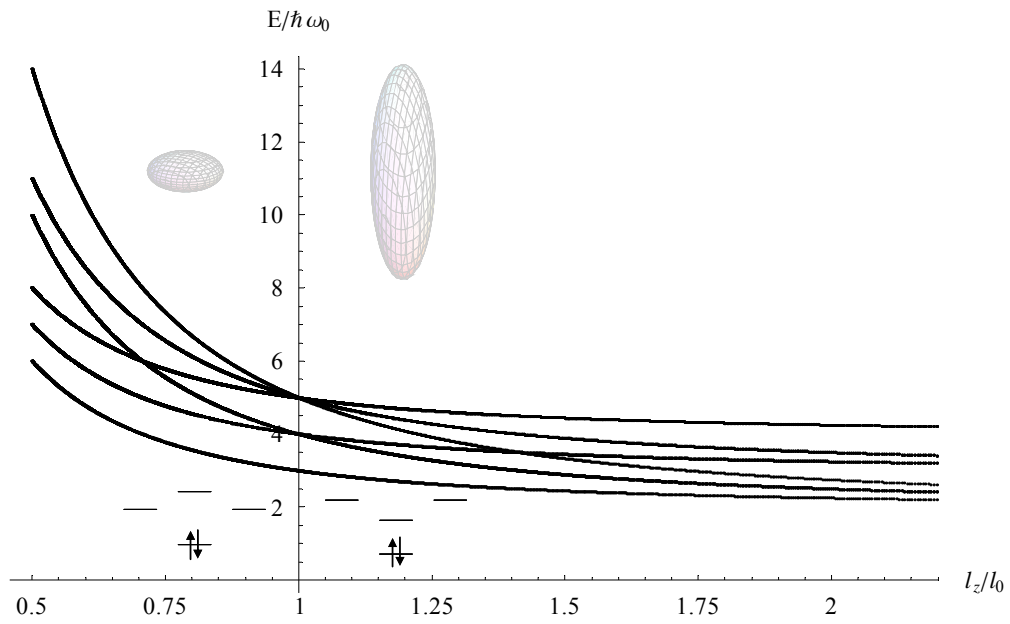


FIG. 4.3.1 Energy spectrum versus aspect ratio where all the possible configurations are considered in the 2-shell approximation when the interaction terms are ignored.

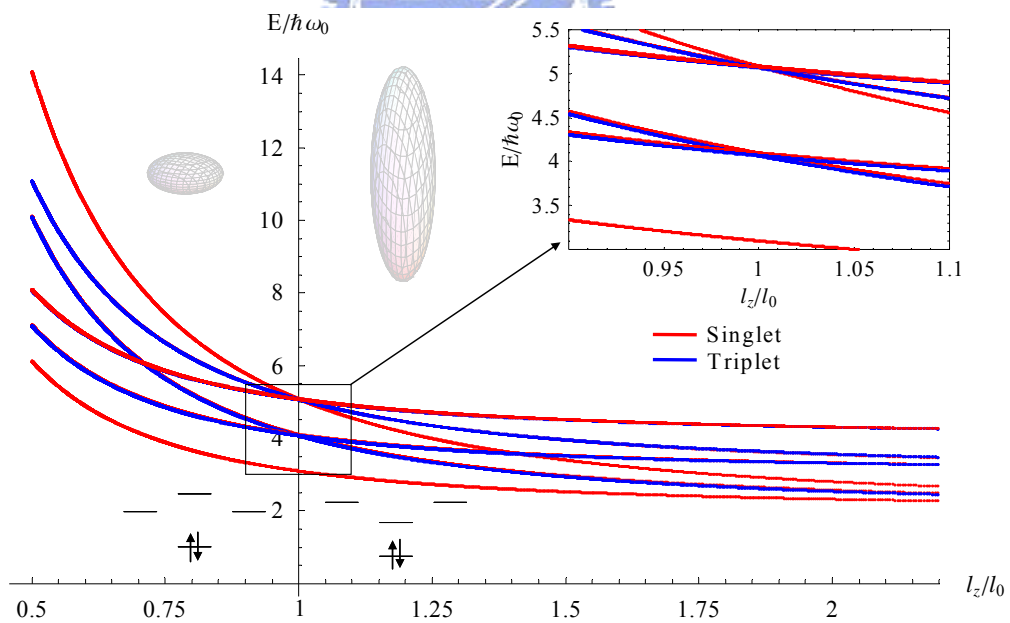


FIG. 4.3.2 Energy spectrum versus aspect ratio, where all the possible configurations are considered in the 2-shell approximation when the interaction terms are included. The state energies decay so rapidly such that the energy difference between singlet and triplet states is not obvious.

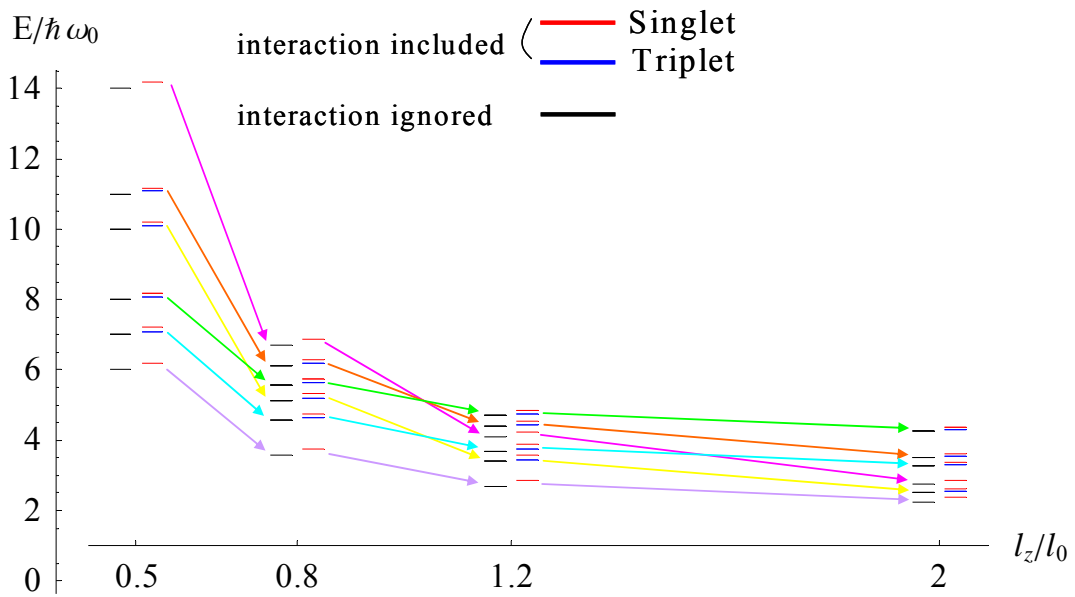


FIG. 4.3.3 Illustration of the energy evolution of each state versus aspect ratio. The evolution can be separated into 4 stages by three critical values of the aspect ratio. At these critical aspect ratios, some excited states cross due to the varying shell structure caused by the anisotropy. Thus the order of the states from low to high energy in each stage is different.

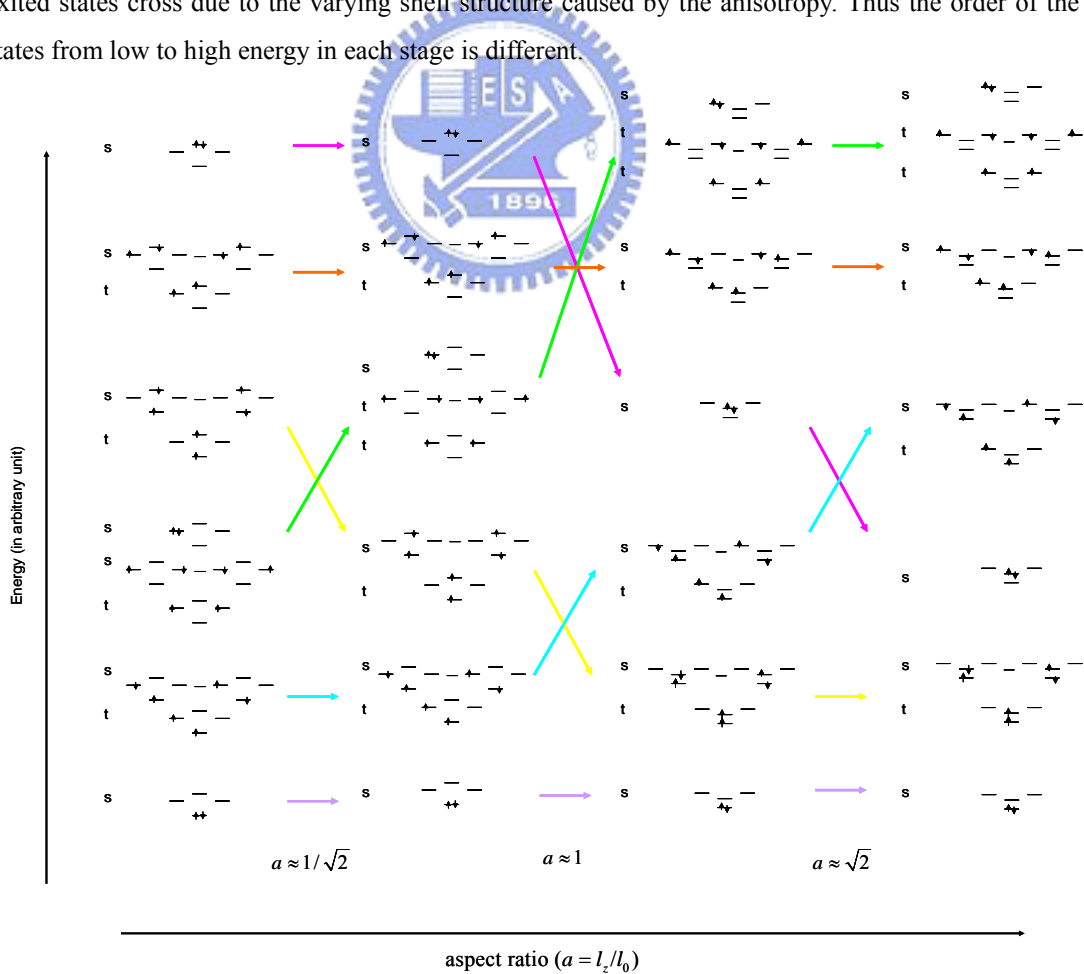


FIG.4.3.4 The evolution of all the states with the aspect ratio. It can be well mapped to FIG.4.3.3, but the energy information is absent. Each transition line is labeled by a different color.

However, the absolute value scale of this difference is the same as that in the nanocrystal when the magnetic field is applied.

The energy evolution of each state with the aspect ratio is a slightly complex. In FIG. 4.3.3 we show the energy evolution of each state versus the aspect ratio. The evolution can be separated into 4 stages by three critical values of the aspect ratio determined by a single particle spectrum. The critical values are approximately $\frac{1}{\sqrt{2}}$, 1, and $\sqrt{2}$, and at these critical values some excited states cross because of the varying shell structure caused by the anisotropy. Thus the order of the states from low to high energy in each stage is different and can be tuned by controlling the aspect ratio. In FIG. 4.3.4 we show the evolution of all the states with the aspect ratio. It contains the complementary information of FIG. 4.3.3 and the transition lines are labeled with different colors. Let us check that does the singlet-triplet transition occur in the ground state. When the system is elongated, the energy of orbital p_0 lowers and the electrons in s probably jump to p_0 . Thus the triplet states we should consider are $|t01\rangle$, $|t02\rangle$, and $|t03\rangle$. The energy spectrum of the ground state and the the first excited state versus the aspect ratio as shown in FIG. 4.3.2 indicates that no transition occurs. We cannot check if the transition occurs with a high aspect ratio because the 2-shell approximation fails in a high anisotropy system. To verify the highly anisotropic conditions, we have to consider more configurations and perform additional calculations. The shell structure of lower states with high aspect ratio is just the 1D SHO states, and thus we should consider the configurations $|0,0,0\rangle$ to $|0,0,q\rangle$. Besides, when the aspect ratio is small, we should take the Fock-Darwin configurations in the calculation. After all, we have demonstrated the 2-electron system in a simplified condition and shown that the electronic structure could be tuned by an external magnetic field and/or the anisotropy.

Chapter 5: Summary

In this thesis we develop a CI theory for interacting electrons in nanostructures with 3D confinement, i.e., nanocrystals and nanorods, based on the 3D parabolic model. We mainly focus on three types of systems: (1) isotropic nanocrystals without magnetic field, (2) isotropic nanocrystals in a magnetic field, and (3) anisotropic nanocrystals (nanorods). As a first step, we demonstrated a two-electron system in the two-shell approximation. We show that one can tailor the electronic structure of NC/NRs and the particle-particle interaction by means of shape-control and applying an external magnetic field; the latter affects the electronic structure slightly while the former results in drastic change of electronic structure and many-body physics.

To obtain numerical results with high accuracy, we should take the number of configurations as many as possible. In practice, we can truncate the Hilbert space spanned by the considered configurations with some cut off energy determined by convergence study. Since the kinetic and interaction terms we derived are universal, the theory we built up could also be applied to describe the behavior of the holes in valence band. Therefore we could study the excitonic problems and explore the optical properties of NC/NR systems. The theory may be applied in other systems such as pillar quantum dots which shapes are similar to NC/NR's such as pillar quantum dots.

In the future, the following subject can be studied as the extended work of this thesis:

1. We may explore the possibility of observing S/T transition by both magnetic field and the breaking of symmetry of NC's.
2. The simple model in this thesis may be compared with the results by atomistic tight-binding theory.
3. The two-electron study may be compared with numerical results.

4. We may explore more-electrons systems by exact diagonalization. The theory is extendable to large scale exact diagonalization calculation.



Appendix: Coulomb Matrix Elements

In this section we will calculate the electron-electron Coulomb energy in the systems discussed in previous chapters. The Coulomb scattering matrix element is denoted by a volume integral

$$\iint d\vec{r}_1 d\vec{r}_2 \left(\psi_i^*(\vec{r}_1) \psi_j^*(\vec{r}_2) \frac{2}{|\vec{r}_1 - \vec{r}_2|} \psi_k(\vec{r}_2) \psi_l(\vec{r}_1) \right) \quad \text{Eq.(A.1),}$$

where $\psi(\vec{r})$ is the wavefunction of single electron, \vec{r}_1 (\vec{r}_2) is the position of electron 1(2), and i, j, k and l are the quantum numbers introduced in chapter 2, i.e.,

$$i = n_1', m_1', s_1'$$

$$j = n_2', m_2', s_2'$$

$$k = n_2, m_2, s_2$$

$$l = n_1, m_1, s_1,$$

The Coulomb interaction operator is $V(\mathbf{r}_1, \mathbf{r}_2) = \frac{2}{|\mathbf{r}_1 - \mathbf{r}_2|}$ which is in the Rydberg unit, and

$\mathbf{r}_1, \mathbf{r}_2$ are in the effective Bohr radius. It should be noted that in the derivation **we use**

quantum number s instead of q for convenience. In our derivation, it is more convenient to express the interaction terms in the Dirac notation

$$\langle ij | V | kl \rangle \equiv \iint d\vec{r}_1 d\vec{r}_2 \left(\psi_i^*(\vec{r}_1) \psi_j^*(\vec{r}_2) \frac{2}{|\vec{r}_1 - \vec{r}_2|} \psi_k(\vec{r}_2) \psi_l(\vec{r}_1) \right) \quad \text{Eq.(A.2).}$$

Further, it is more convenient to calculate the matrix elements in the reciprocal space. In 3D systems the Coulomb potential can be written as the Fourier series

$$v = \sum_q v_q e^{i\mathbf{q} \cdot (\mathbf{r}_1 - \mathbf{r}_2)} \quad \text{Eq.(A.3),}$$

where $v_q = \frac{8\pi}{q^2}$ and $\mathbf{q} = (q_x, q_y, q_z)$.

Then the matrix element becomes

$$\langle ij | V | kl \rangle = \sum_q \frac{8\pi}{q^2} \langle i | e^{i\mathbf{q} \cdot \mathbf{r}_1} | l \rangle \langle j | e^{-i\mathbf{q} \cdot \mathbf{r}_2} | k \rangle = \sum_q \frac{8\pi}{q^2} M_1 M_2 \quad \text{Eq.(A.4),}$$

Here we let $M_1 = \langle i | e^{i\mathbf{q} \cdot \mathbf{r}_1} | l \rangle$ and $M_2 = \langle j | e^{-i\mathbf{q} \cdot \mathbf{r}_2} | k \rangle$.

From the above definition, we have the operators

$$\begin{aligned} x &= \frac{l}{\sqrt{2}}(a + a^+ + b + b^+), \\ y &= \frac{il}{\sqrt{2}}(a - a^+ - b + b^+), \\ z &= l_z(c + c^+). \end{aligned} \tag{A.5}$$

All the operators $a^{(+)}$, $b^{(+)}$, $c^{(+)}$ and parameters l , l_z are defined in chapter 2.

Before calculating M_1 , we must deal with $e^{i\mathbf{q}\cdot\mathbf{r}_1}$:

$$\begin{aligned} e^{i\mathbf{q}\cdot\mathbf{r}_1} &= e^{i(q_x x_1 + q_y y_1 + q_z z_1)} \\ &= e^{i\left[\frac{lq_x}{\sqrt{2}}(a_1 + a_1^+ + b_1 + b_1^+) + \frac{ilq_y}{\sqrt{2}}(a_1 - a_1^+ - b_1 + b_1^+) + q_z l_z (c_1 + c_1^+)\right]} \\ &= e^{i(a_1 Q_p + a_1^+ Q_p^* + b_1 Q_p + b_1^+ Q_p^* + c_1 Q_z + c_1^+ Q_z)} \end{aligned} \tag{A.6}$$

with the definition

$$\begin{aligned} Q_p &= \frac{l}{\sqrt{2}}(q_x + iq_y), \\ Q_z &= l_z q_z. \end{aligned}$$



In order to disentangle the operators in the exponent, we use the Trotter-Suzuki formula

$$e^{\hat{A} + \hat{B}} = e^{\hat{A}} e^{\hat{B}} e^{-\frac{1}{2}[\hat{A}, \hat{B}]} \tag{A.7}$$

which is applicable under the condition $[\hat{A}, [\hat{A}, \hat{B}]] = [\hat{B}, [\hat{A}, \hat{B}]] = 0$. With this formula we may write $e^{i\mathbf{q}\cdot\mathbf{r}_1}$ as

$$e^{i\mathbf{q}\cdot\mathbf{r}_1} = e^{-|Q_p|^2} e^{iQ_p^* a_1^+} e^{iQ_p a_1} e^{iQ_p b_1^+} e^{iQ_p^* b_1} e^{-\frac{|Q_z|^2}{2}} e^{iQ_z c_1^+} e^{iQ_z c_1} \tag{A.8}$$

Then we can calculate M_1 as follows:

$$\begin{aligned}
M_1 &= \langle i | e^{ik \cdot \mathbf{r}_1} | l \rangle \\
&= \langle i | e^{-iQ_\rho l^2} e^{iQ_\rho^* a_1^+} e^{iQ_\rho a_1} e^{iQ_\rho b_1^+} e^{iQ_\rho^* b_1} e^{-\frac{|Q_z l^2}{2}} e^{iQ_z c_1^+} e^{iQ_z c_1} | l \rangle \\
&= \frac{e^{-i(Q_\rho l^2 + \frac{|Q_z l^2}{2})}}{\sqrt{n_1! m_1! s_1! n_1! m_1! s_1!}} \\
&\quad \times \langle 000 | c_1^{q_1} b_1^{m_1} a_1^{n_1} e^{iQ_\rho^* a_1^+} e^{iQ_\rho b_1^+} e^{iQ_z c_1^+} \hat{\mathbf{I}} e^{iQ_\rho a_1} e^{iQ_\rho^* b_1} e^{iQ_z c_1} (a_1^+)^{n_1} (b_1^+)^{m_1} (c_1^+)^{s_1} | 000 \rangle \\
&= \frac{e^{-i(Q_\rho l^2 + \frac{|Q_z l^2}{2})}}{\sqrt{n_1! m_1! s_1! n_1! m_1! s_1!}} \langle 000 | c_1^{q_1} b_1^{m_1} a_1^{n_1} e^{iQ_\rho^* a_1^+} e^{iQ_\rho b_1^+} e^{iQ_z c_1^+} \\
&\quad \times \sum_{p_1=0}^{\infty} \sum_{p_2=0}^{\infty} \sum_{p_3=0}^{\infty} \left(\frac{1}{p_1! p_2! p_3!} (a_1^+)^{p_1} (b_1^+)^{p_2} (c_1^+)^{p_3} | 000 \rangle \langle 000 | (a_1)^{p_1} (b_1)^{p_2} (c_1)^{p_3} \right) \\
&\quad \times e^{iQ_\rho a_1} e^{iQ_\rho^* b_1} e^{iQ_z c_1} (a_1^+)^{n_1} (b_1^+)^{m_1} (c_1^+)^{s_1} | 000 \rangle \\
&= \frac{e^{-i(Q_\rho l^2 + \frac{|Q_z l^2}{2})}}{\sqrt{n_1! m_1! s_1! n_1! m_1! s_1!}} \sum_{p_1=0}^{\min(n_1', n_1)} \sum_{p_2=0}^{\min(m_1', m_1)} \sum_{p_3=0}^{\min(s_1', s_1)} \\
&\quad [p_1! p_2! p_3! \binom{n_1'}{p_1} \binom{n_1}{p_1} \binom{m_1'}{p_2} \binom{m_1}{p_2} \binom{s_1'}{p_3} \binom{s_1}{p_3} \\
&\quad \times (iQ_\rho^*)^{n_1' - p_1} (-iQ_\rho)^{m_1' - p_2} (iQ_z)^{s_1' - p_3} (iQ_\rho)^{n_1 - p_1} (iQ_\rho^*)^{m_1 - p_2} (iQ_z)^{s_1 - p_3}]
\end{aligned} \tag{A.9}$$

Similarly, we have

$$\begin{aligned}
M_2 &= \langle j | e^{-iq \cdot \mathbf{r}_2} | k \rangle \\
&= \frac{e^{-i(q_\rho l^2 + \frac{|q_z l^2}{2})}}{\sqrt{n_2! m_2! q_2! n_2! m_2! q_2!}} \sum_{p_4=0}^{\min(n_2', n_2)} \sum_{p_5=0}^{\min(m_2', m_2)} \sum_{p_6=0}^{\min(s_2', s_2)} \\
&\quad [p_4! p_5! p_6! \binom{n_2'}{p_4} \binom{n_2}{p_4} \binom{m_2'}{p_5} \binom{m_2}{p_5} \binom{s_2'}{p_6} \binom{s_2}{p_6} \\
&\quad \times (-iQ_\rho^*)^{n_2' - p_4} (-iQ_\rho)^{m_2' - p_5} (-iQ_z)^{s_2' - p_6} (-iQ_\rho)^{n_2 - p_4} (-iQ_\rho^*)^{m_2 - p_5} (-iQ_z)^{s_2 - p_6}]
\end{aligned} \tag{A.10}$$

Now we can calculate the scattering matrix elements. Replacing the summation over plane waves by an integral, the matrix elements become

$$\langle ij | V | kl \rangle = \frac{1}{8\pi^3} \int_0^\infty q_\rho dq_\rho \int_0^{2\pi} d\phi_q \int_{-\infty}^\infty dq_z \left(\frac{8\pi}{q^2} M_1 M_2 \right) \tag{A.11},$$

where q_ρ , ϕ_q , and q_z are the three cylindrical coordinates in the reciprocal space. By the

definition $Q_p = \frac{l}{\sqrt{2}}(q_x + iq_y)$, we have $Q_p = \frac{l}{\sqrt{2}}(q_\rho e^{i\phi_q})$. With M_1 and M_2 obtained

above, the integral can be arranged more systematically

$$\begin{aligned}
\langle ij | V | kl \rangle = & \frac{1}{\pi^2 \sqrt{n_1'! m_1'! s_1'! n_1! m_1! s_1! n_2'! m_2'! s_2'! n_2! m_2! s_2!}} \\
& \times \sum_{p_1=0}^{\min(n_1', n_1)} \sum_{p_2=0}^{\min(m_1', m_1)} \sum_{p_3=0}^{\min(s_1', s_1)} \sum_{p_4=0}^{\min(n_2', n_2)} \sum_{p_5=0}^{\min(m_2', m_2)} \sum_{p_6=0}^{\min(s_2', s_2)} \{p_1! p_2! p_3! p_4! p_5! p_6! \\
& \times \binom{n_1'}{p_1} \binom{n_1}{p_1} \binom{m_1'}{p_2} \binom{m_1}{p_2} \binom{s_1'}{p_3} \binom{s_1}{p_3} \binom{n_2'}{p_4} \binom{n_2}{p_4} \binom{m_2'}{p_5} \binom{m_2}{p_5} \binom{s_2'}{p_6} \binom{s_2}{p_6} \\
& \times (-1)^{n_2'+m_2'+s_2'+n_2+m_2+s_2} \times l^{n_1'+m_1'+s_1'+n_1+m_1+s_1+n_2'+m_2'+s_2'+n_2+m_2+s_2-2(p_1+p_2+p_3+p_4+p_5+p_6)} \\
& \times \left(\frac{l}{\sqrt{2}}\right)^{n_1'+m_1'+n_1+m_1+n_2'+m_2'+n_2+m_2-2(p_1+p_2+p_4+p_5)} \times I_z^{s_1'+s_1+s_2'+s_2-2(p_3+p_6)} \\
& \times \int_0^\infty q_\rho dq_\rho \int_0^{2\pi} d\phi_q \int_{-\infty}^\infty dq_z \left[\frac{e^{-(l^2 q_\rho^2 + l_z^2 q_z^2)}}{q_\rho^2 + q_z^2} q_\rho^{1+n_1'+m_1'+n_1+m_1+n_2'+m_2'+n_2+m_2-2(p_1+p_2+p_4+p_5)} \right. \\
& \left. \times (e^{i\phi_q})^{m_1'+m_2'+n_1+n_2-(n_1'+n_2'+m_1+m_2)} \times q_z^{q_1'+q_1+q_2'+q_2-2(p_3+p_6)} \right] \} \quad \text{Eq.(A.12),}
\end{aligned}$$

The most serious problem is posed by the volume integral. First we perform the integration of the angular part which is obviously quite simple,

$$\int_0^{2\pi} (e^{i\phi_q})^{m_1'+m_2'+n_1+n_2-(n_1'+n_2'+m_1+m_2)} d\phi_q = 2\pi \delta_{R_L, R_R} \quad \text{Eq.(A.13),}$$

where $R_L = (m_1' + m_2') - (n_1' + n_2')$ and $R_R = (m_1 + m_2) - (n_1 + n_2)$. The delta function reflects the fact that the \mathbf{z} -component of the angular momentum is conserved since the vector potential corresponding to the magnetic field in the \mathbf{z} direction is on the x-y plane and has no influence in the \mathbf{z} direction.

Now the last problem is the 2D integral. We first consider the simplest case where the system is isotropic and under no magnetic field. Under this condition, by changing the variables, we have

$$\begin{aligned}
\langle ij | V | kl \rangle = & \frac{\delta_{R_L, R_R} \cdot \delta_{s_1'+s_1+s_2'+s_2, \text{even}}}{\pi l_0 \sqrt{n_1! m_1! s_1! n_1! m_1! s_1! n_2! m_2! s_2! n_2! m_2! s_2!}} \\
& \times \sum_{p_1=0}^{\min(n_1', n_1)} \sum_{p_2=0}^{\min(m_1', m_1)} \sum_{p_3=0}^{\min(s_1', s_1)} \sum_{p_4=0}^{\min(n_2', n_2)} \sum_{p_5=0}^{\min(m_2', m_2)} \sum_{p_6=0}^{\min(s_2', s_2)} \{p_1! p_2! p_3! p_4! p_5! p_6!\} \\
& \times \binom{n_1'}{p_1} \binom{n_1}{p_1} \binom{m_1'}{p_2} \binom{m_1}{p_2} \binom{s_1'}{p_3} \binom{s_1}{p_3} \binom{n_2'}{p_4} \binom{n_2}{p_4} \binom{m_2'}{p_5} \binom{m_2}{p_5} \binom{s_2'}{p_6} \binom{s_2}{p_6} \\
& \times (-1)^{u+v+n_2'+m_2-n_2-m_2'+s_2'+s_2} \times \left(\frac{1}{2}\right)^u \\
& \times \frac{\Gamma(1+u)\Gamma\left(\frac{1}{2}+v\right)\Gamma\left(\frac{1}{2}+u+v\right)}{\Gamma\left(\frac{3}{2}+u+v\right)} \}
\end{aligned} \tag{A.14}$$

where $u = m_1' + m_2' + n_1 + n_2 - (p_1 + p_2 + p_4 + p_5)$,

$$v = \frac{s_1' + s_1 + s_2' + s_2}{2} - (p_3 + p_6).$$

Note that $\langle ij | V | kl \rangle \neq 0$ only when v is an integer, which means $s_1' + s_1 + s_2' + s_2$ must be even. If $s_1 + s_2$ is even (odd), $s_1' + s_2'$ must also be even (odd). This selection rule reveals that the parity of the colliding electrons states should be conserved.

If the system is under a magnetic field and (or) not isotropic in the \mathbf{z} direction, the scattering matrix elements become slightly more complicated:

$$\begin{aligned}
\langle ij | V | kl \rangle = & \frac{\delta_{R_L, R_R} \cdot \delta_{s_1'+s_1+s_2'+s_2, \text{even}}}{\pi l_z \sqrt{n_1! m_1! s_1! n_1! m_1! s_1! n_2! m_2! s_2! n_2! m_2! s_2!}} \\
& \times \sum_{p_1=0}^{\min(n_1', n_1)} \sum_{p_2=0}^{\min(m_1', m_1)} \sum_{p_3=0}^{\min(s_1', s_1)} \sum_{p_4=0}^{\min(n_2', n_2)} \sum_{p_5=0}^{\min(m_2', m_2)} \sum_{p_6=0}^{\min(s_2', s_2)} \{p_1! p_2! p_3! p_4! p_5! p_6!\} \\
& \times \binom{n_1'}{p_1} \binom{n_1}{p_1} \binom{m_1'}{p_2} \binom{m_1}{p_2} \binom{s_1'}{p_3} \binom{s_1}{p_3} \binom{n_2'}{p_4} \binom{n_2}{p_4} \binom{m_2'}{p_5} \binom{m_2}{p_5} \binom{s_2'}{p_6} \binom{s_2}{p_6} \\
& \times (-1)^{u+v+n_2'+m_2-n_2-m_2'+s_2'+s_2} \times \left(\frac{\omega_z}{2\omega_h}\right)^u \\
& \times \frac{\Gamma(1+u)\Gamma\left(\frac{1}{2}+v\right)\Gamma\left(\frac{1}{2}+u+v\right)}{\Gamma\left(\frac{3}{2}+u+v\right)} \times {}_2F_1\left(1+u, \frac{1}{2}+u+v; \frac{3}{2}+u+v; 1-\frac{\omega_z}{\omega_h}\right) \}
\end{aligned} \tag{A.15}$$

where ${}_2F_1$ is the hypergeometric function. ${}_2F_1\left(1+u, \frac{1+2u+v}{2}; \frac{3+2u+v}{2}; 0\right) = 1$ recovers

the isotropic and no magnetic field case (Eq.(A.14)).



References

1. A. P. Alivisatos, "Semiconductor clusters, nanocrystals, and quantum dots", *Science*, **271**, 933 (1996).
2. U. Banin and O. Millo, "Tunneling and optical spectroscopy of semiconductor nanocrystals", *Annual Review of Physical Chemistry*, **54**, 465 (2003).
3. V. I. Klimov, A. A. Mikhailovsky, S. Xu, A. Malko, J. A. Hollingsworth, C. A. Leatherdale, H.-J. Eisler, and M. G. Bawendi, "Optical gain and stimulated emission in nanocrystal quantum dots", *Science*, **290**, 314 (2000).
4. M. Bruchez, Jr., M. Moronne, P. Gin, S. Weiss, and A. P. Alivisatos, "Semiconductor nanocrystals as fluorescent biological labels", *Science*, **281**, 2013 (1998).
5. L. Brus, "Quantum crystallites and nonlinear optics", *Applied Physics A*, **53**, 465 (1991).
6. N. Tessler, V. Medvedev, M. Kazes, S. Kan, and U. Banin, "Efficient near-infrared polymer nanocrystal light-emitting diodes", *Science*, **295**, 1506 (2002).
7. U. Banin, Y. Cao, D. Katz, and O. Millo, "Identification of atomic-like electronic states in indium arsenide nanocrystal quantum dots", *Nature*, **400**, 542 (1999).
8. E. P. Bakkers and D. Vanmaekelbergh, "Resonant electron tunneling through semiconducting nanocrystals in a symmetrical and an asymmetrical junction", *Physical Review B*, **62**, 7743 (2000).
9. S. A. Empedocles, D. J. Norris, and M. G. Bawendi, "Photoluminescence spectroscopy of single CdSe nanocrystallite quantum dots", *Physical Review Letters*, **77**, 3873 (1996).
10. J. Hu, L. Li, W. Yang, L. Manna, L. Wang, and A. P. Alivisatos, "Linearly polarized emission from colloidal semiconductor quantum rods", *Science*, **292**, 2060 (2001).
11. I. G. Ivanov, B. Magnusson, and E. Janzen, "Optical selection rules for shallow donors in 4H-SiC and ionization energy of the nitrogen donor at the hexagonal site", *Physical Review B*, **67**, 165212 (2003).
12. P. Chen, "Quantum shape effects on Zeeman splittings in semiconductor nanostructures", *Physical Review B*, **72**, 045335 (2005).

13. A. J. Williamson and A. Zunger, "Pseudopotential study of electron-hole excitations in colloidal free-standing InAs quantum dots", *Physical Review B*, **61**, 1978 (2000).
14. Kouwenhoven and McEuen, "*Nanotechnology*", edited by G. Timp (Springer, New York) p. 471 (1999).
15. Y. Tanaka and H. Akerai, "Many-body effects in transport through a quantum dot", *Physical Review B*, **53**, 3901 (1996).
16. P. L. McEuen, E. B. Foxman, J. Kinaret, U. Meirav, M. A. Kastner, N. S. Wingreen, S. J. Wind, "Self-consistent addition spectrum of a Coulomb island in the quantum Hall regime", *Physical Review B*, **45**, 11419 (1992).
17. R. C. Ashoori, H. L. Stormer, J. S. Weiner, L. N. Pfeiffer, K. W. Baldwin, K. W. West, "*N*-electron ground state energies of a quantum dot in magnetic field", *Physical Review Letters*, **71**, 613 (1993).
18. T. H. Oosterkamp, J. W. Janssen, L. P. Kouwenhoven, D. G. Austing, T. Honda, and S. Tarucha, "Maximum-Density droplet and charge redistributions in quantum dots at high magnetic fields", *Physical Review Letters*, **82**, 2931 (1999).
19. P. Hawrylak, "Excitonic artificial atoms: Engineering optical properties of quantum dots", *Physical Review B*, **60**, 5597 (1999).
20. C. B. Murray, S. Sun, W. Gaschler, H. Doyle, T. A. Betley, C. R. Kagan, "Colloidal synthesis of nanocrystals and nanocrystal superlattices", *IBM Journal of Research and Development*, **45**, No.1 (2001).